# DEVELOPMENT AND COMPUTATIONAL EVALUATION OF DUAL-PEAK DOUBLE PLASMONIC-LAYERED PCF SENSOR

by

**Shihab Shahriar (190021123)**
**Fahima Shahana Rahman (190021138)**
**Sumaiya Tasnim Adiba (190021201)**


Department of Electrical and Electronic Engineering
**Islamic University of Technology (IUT)**
Gazipur, Bangladesh

June 2024

# DEVELOPMENT AND COMPUTATIONAL EVALUATION OF DUAL-PEAK DOUBLE PLASMONIC-LAYERED PCF SENSOR

Approved by:

---

**Prof. Dr. Mohammad Rakibul Islam**

Supervisor and Professor,
Department of Electrical and Electronic Engineering,
Islamic University of Technology (IUT),
Boardbazar. Gazipur-1704.

Date: .....04-07-24

# DECLARATION OF AUTHORSHIP

By signing this document, Shihab Shahriar (180021123), Fahima Shahana Rahman (180021138), and Sumaiya Tasnim Adiba (180021201) affirm that the content in the thesis book " Development and Computational Evaluation of Dual-Peak Double Plasmonic-Layered PCF Sensor" is the product of our combined original work and individual efforts.

## Signatures of Students

Shihab Shahriar
ID 190021123

04.07.24

Fahima Shahana Rahman
ID 190021138

04-07-24

Sumaiya Tasnim Adiba
ID 190021201

# ABSTRACT

The design and numerical analysis of a dual-peak plasmonic multilayer Photonic Crystal Fiber (PCF) sensor are presented in this thesis. PCFs are perfect for sophisticated sensing applications because of their remarkable control over light propagation, which stems from their unique microstructured construction. The sensor achieves great sensitivity to changes in refractive index by utilizing Surface Plasmon Resonance (SPR), which makes use of the resonant oscillation of conduction electrons at a metal-dielectric interface. Throughout the near-infrared (NIR) spectrum, the suggested sensor exhibits remarkable performance parameters, such as high wavelength and amplitude sensitivity. This work highlights the promise of dual-peak plasmonic multilayer PCF sensors in applications like biosensing, environmental monitoring, and telecommunications through meticulous structural optimization and material selection.

# Table of Contents

# List of Tables

# List of Figures

# List of Acronyms

LSPR: Localized Surface Plasmon Resonance

PCF: Photonic Crystal Fiber

EMF: Electromagnetic Field

SPW: Surface Plasmon Wave

FOM: Figure of Merit

AS: Amplitude Sensitivity

PML: Perfectly Matched Layer

RIU: Refractive Index Unit

THz: Terahertz

SP: Surface Plasmon

ER: Extinction Ratio

CLR: Confinement Loss Ratio

SPP: Surface Plasmon Polariton

TE: Transverse Electric

TM: Transverse Magnetic

WS: Wavelength Sensitivity

CT: Crosstalk

RS: Relative Sensitivity

SPR: Surface Plasmon Resonance

NIR: Near-infrared Region

GZO: Gallium doped Zinc Oxide

TIR: Total Internal Reflection

CL: Confinement Loss

# Chapter 1

# Introduction

## 1.1 Background

In the past few decades, there have been remarkable developments in photonics—the study of light and its interaction with matter—which have radically changed a number of scientific and industrial disciplines. One of the most revolutionary developments in this field is the creation of photonic crystal fibers (PCFs). By providing unmatched control over light propagation, PCFs have immensely altered the field of optical fibers and made a wide range of cutting-edge applications possible that were previously impossible with traditional optical fibers.

PCFs are based on the idea of photonic crystals, which was first presented in the late 1980s. These structures display periodic fluctuations in dielectric on the wavelength scale, resulting in a photonic bandgap that can prevent some wavelengths from propagating. Soon after, this ground-breaking concept was applied to optical fibers, which resulted in the early 1990s PCF proposal. Leading researchers in this field, Philip Russell and colleagues at the University of Bath demonstrated the first usable PCF in 1996, making them among the pioneers in the field. fibers.

PCFs have come a long way since they were first developed, thanks to both theoretical and experimental advances. Early PCFs were primarily concerned with elucidating fundamental guiding processes and their underlying characteristics. Researchers started experimenting with more intricate designs and materials as fabrication techniques advanced, which resulted in the creation of PCFs with enhanced confinement, highly nonlinear characteristics, and customized dispersion.

The creation of infinitely single-mode fibers was a crucial turning point in the development of PCFs. These fibers are essential in applications that need steady and reliable single-mode operation, like high-precision metrology and high-resolution spectroscopy. They are distinguished by their capacity to support only one mode over a wide wavelength range.
The development of hollow-core PCFs was a significant advancement. By minimizing the interface between the directed light and the fiber material, these fibers enable sensitive gas

sensing and high-power applications while also significantly lowering losses. Researchers have also looked into other doping methods and materials to improve PCF performance even more, extending its operating range from the visible to the M-IR (mid-infrared) spectrum.

PCFs are at the forefront of optical fiber technology today, with a wide range of uses. PCFs are used in telecommunications to increase network stability and data transfer speeds. Their capacity to accurately manage nonlinearity and dispersion makes them indispensable for the creation of supercontinuum light sources, which are necessary for many applications in science and medicine.

PCFs have made it possible to create extremely sensitive sensors in the sensing field that can pick up on even the smallest changes in the surrounding environment. Their microstructured design facilitates applications in industrial process control, biomedical diagnostics, and environmental monitoring by allowing the insertion of different sensing elements, such gases or liquids, within the fiber structure.

The increasing need for sophisticated optical devices with improved performance and additional features is what propels PCF technology's ongoing evolution. To push the limits of what PCFs can accomplish and solve new problems, researchers are continually investigating innovative designs and materials. This will allow for the discovery of new applications.

The creation of a unique exposed core LSPR-PCF sensor in the shape of a wheel is a noteworthy development in this regard. By optimizing the interaction between light and the accompanying medium, this novel design seeks to enhance sensitivity and expand the operational bandwidth. This research aims to contribute to the continuous advancement of photonic crystal fiber technology by utilizing the special qualities of PCFs and incorporating sophisticated sensing mechanisms, offering reliable solutions for optical communication, mid-infrared sensing, and biosensing applications.

## 1.2 Problem Statement

While major advancements have been conducted in the field of Localized Surface Plasmon Resonance (LSPR) integrated Photonic Crystal Fiber (PCF) sensors, a number of significant obstacles remain in the way of their broad implementation and efficiency. These difficulties include restrictions on operational bandwidth, robustness, dependability, sensitivity, and the difficulty of obtaining dual-peak sensing. For LSPR-PCF sensors to advance in high-impact applications including optical communication, environmental monitoring, and medical diagnostics, these challenges must be overcome.

- **Restricted Sensitivity**

Current LSPR-PCF sensors frequently lack the high sensitivity needed to identify analytes at low concentrations, which is crucial for environmental monitoring and medical diagnostics. Accurately detecting and quantifying minute changes in target analytes requires both PCF structure optimization and the amplification of the local electromagnetic field surrounding metallic nanoparticles to reach the appropriate sensitivity levels.

- **Limited Functional Bandwidth**

The restricted operating bandwidths of many of the LSPR-PCF sensors now in use limit their adaptability and usefulness in a wide range of spectrum areas. Applications requiring broad-spectrum sensing, such multi-wavelength biomedical imaging and telecommunications, find this limitation especially troublesome. A larger operational bandwidth would allow the sensor to function well over a variety of spectral areas, including visible, near-infrared (NIR), and mid-infrared (M-IR) bands, and detect a greater range of analytes

- **Sturdiness and Dependability**

Another major problem is ensuring constant and reliable sensor performance in real-world, practical situations. Environmental variations that can have a major impact on sensor performance include changes in temperature, humidity, and mechanical vibrations. As a result, robust and stable sensor designs are required to retain high performance and accuracy in the face of environmental fluctuations.

- **Intricacy of Dual-Peak Sensing Systems**

Although it is technically difficult, achieving dual-peak sensing is essential to improving sensor performance. By providing redundant readings, dual-peak sensing lowers false positives and

boosts reliability. It is necessary to precisely manage the optical characteristics and resonance conditions, optimize the PCF structure to allow dual-peak responses, and fine-tune the metallic nanoparticles to generate stable and distinct resonance peaks in order to design a sensor that can do this.

To enhance SPR sensor technology, these challenges and limitations must be addressed. To fully utilize SPR sensors in a variety of sensing applications, researchers ought to concentrate on three main objectives: streamlining the fabrication process, increasing sensitivity through enhanced evanescent field characteristics, and lowering the total cost.

## 1.3 Purpose Behind the Research

The necessity to address important issues with existing photonic sensing technology, specifically with regard to integrated Photonic Crystal Fiber (PCF) sensors that are Localized Surface Plasmon Resonance (LSPR), is what motivates this research. Due to their severe sensitivity, operational bandwidth, and reliability constraints, these sensors are not widely used or as successful in a wide range of applications, including optical communication, monitoring of environment, and medical diagnostics.

- **Design Enhancement**

The development of an optimal design for an exposed core LSPR-PCF sensor in the form of a wheel is one of the main goals. By carefully adjusting sensor geometry and material qualities, this design seeks to maximize sensitivity and operating bandwidth. Iteratively enhancing the light-environment interaction, sophisticated modeling techniques are used to improve performance over a range of spectral areas, from visible light to mid-infrared region.

- **Realizing Dual-Peak Sensing**

By offering redundant readings, achieving dual-peak sensing capabilities is essential for improving sensor dependability. Precise tailoring of the LSPR characteristics and optical qualities is required to achieve this goal. Stable and identifiable dual peaks in the sensor's spectral response require fine tuning of the nanoparticle's size, shape, and material composition. This kind of capacity lowers the probability of false positives, which is important for demanding applications in environmental monitoring and diagnostics, while also improving sensitivity to even the smallest changes in the surroundings.

- **Assessment of Applications**

Key domains covered by the evaluation include biosensing, the M-IR region, and optical communication bands. Extensive calculations and experimental validations are carried out to evaluate the sensor's performance in identifying pertinent analytes in a variety of spectral bands. To show resilience and reliability in real-world circumstances, rigorous testing is conducted under a plethora of environmental variables, including temperature, humidity, and atmospheric pressure. The assessments provide valuable insights that guide future improvements to sensor design, which in turn facilitate their practical implementation and effective integration in many industrial and biological applications.

- **Importance and Contributions**

By creating a strong and adaptable instrument that can sense at two different peak positions, our research aims to further the field of photonic sensing technology. Through the expansion of its operational capabilities and the surmounting of existing constraints, the wheel-shaped exposed core LSPR-PCF sensor is intended to stimulate innovation in both scientific and industrial fields. Expected results include increased sensitivity, wider operating spectrum, and increased dependability, which will promote revolutionary progress and solve urgent issues in optical sensing technology.

## 1.4 Motivation Behind the Research

The increasing need for sophisticated sensing technology in several industries is what spurred this research work of ours. The necessity for creative sensor designs is highlighted by the following elements in particular:

- **Optical Communications**

To improve the functionality and effectiveness of fiber optic networks, the field of optical communications is constantly in need of more sensitive and dependable sensors. Retaining high-speed data transmission and network stability requires accurate sensing of environmental changes and signal distortion.

- **Mid-Infrared (M-IR) Sensing**

Applications like industrial process control, medical diagnostics, and environmental monitoring are highly interested in the M-IR region. This spectral region requires extremely

sensitive sensors that can identify a variety of materials, such as gasses and biological compounds.

- **Biosensing**

Early disease diagnosis and disease monitoring depend on the biomedical field's capacity to identify low concentrations of biological analytes. The sensitivity and specificity of traditional sensors are frequently insufficient, underscoring the need for more sophisticated systems that can satisfy these demanding specifications.

## 1.5 Framework of the Thesis

Following is a breakdown of the contents of this thesis book and what each chapter entails, one by one:

- **Chapter 2** delves into Photonic Crystal Fibers (PCFs), detailing their structural analysis and various categories. It covers the classification of structural designs, light-guiding mechanisms, key characteristics, fabrication methods, and the advantages of PCFs over traditional optical fibers. This chapter also discusses the applications of PCFs.
- **Chapter 3** introduces Surface Plasmon Resonance (SPR), explaining its working mechanism, including Surface Plasmon Wave (SPW), evanescent fields, and confinement loss. The chapter highlights the benefits of SPR, its implementation, and limitations. It also introduces Localized Surface Plasmon Resonance (LSPR), comparing it with SPR, and discusses its working mechanism, implementation, and limitations.
- **Chapter 4** focuses on the sensing mechanisms and plasmonic materials used in sensors. It outlines the prism-based approach, internal and external sensing sensors, and the rationale for using PCF in SPR. The chapter introduces different plasmonic materials, their infusion in PCF-SPR sensors, and factors to consider when choosing plasmonic materials for designing real-life sensors.
- **Chapter 5** provides an overview of the research on PCF-SPR sensors, summarizing the key findings and developments in this field.
- **Chapter 6** presents the proposed design of a novel wheel-like open-core PCF sensor for sensing double peaks. It describes the sensor's structure, specifications, materials

used, dispersion properties, and optimization of sensor parameters, including the widths of the ITO, Ag, and TiO2 layers, as well as the air hole width and pitch.

- **Chapter 7** analyzes the performance parameters of the presented sensor, including Double Peak Sensing Sensitivity (DPSS), wavelength sensitivity (WS), amplitude sensitivity (AS), sensor resolution, linearity, and figure of merit (FOM).
- **Chapter 8** discusses the applications and novelty of the proposed sensor. It highlights its utilization in the mid-infrared (M-IR) region and optical communication bands, potential in bio-sensing, and compares the sensor with relevant past work.
- **Chapter 9** details the fabrication methods of the sensor, including the stack and draw method, CNC drilling, double-step photolithography, and chemical vapor deposition.
- **Chapter 10** outlines the future work plan and provides concluding remarks. It discusses potential future directions for research and summarizes the key findings and contributions of the study.
- **Chapter 11** demonstrates the outcome-based education (OBE) approach, addressing course outcomes (COs), program outcomes (POs), knowledge profiles (K3 – K8), and attributes of ranges of complex engineering problem-solving (P1 – P7) and complex engineering activities (A1 – A5).

# Chapter 2

# Delving into PCFs: Photonic Crystal Fibers

## 2.1 Introduction

One of the biggest developments in optical fiber technology since the creation of the ordinary optical fiber is the application of photonic crystal fibers, or PCFs. PCFs, which were first introduced in the late 1990s, have completely changed the field of photonics because of their exceptional microstructured designs, which provide unmatched control over light propagation. In contrast to conventional optical fibers, PCFs have a periodic array of air holes or other materials throughout their length to guide light instead of depending on a homogeneous core and cladding construction. This novel structure makes it possible to precisely manipulate light, which opens up a wide range of applications in sensing, industrial processing, medical diagnostics, and telecommunications.

PCF development has been characterized by ongoing innovation and improvement. Early designs were centered on single-mode functioning and low loss, but as fabrication methods advanced, scientists started looking at more intricate structures with special optical qualities. The development of fibers with customized dispersion, strong nonlinearity, and the capacity to direct light in unusual ways—such as through hollow cores or photonic bandgaps—has been made possible by the design freedom.

Supercontinuum light sources, solitons, and other nonlinear phenomena can be produced using PCFs' high nonlinearity and adjustable dispersion, which has created new opportunities in the field of nonlinear optics. PCFs are used in telecommunications to produce fibers with customized dispersion profiles and ultra-low loss, enhancing the functionality and capacity of optical communication networks. When it comes to sensing, PCFs are perfect for precisely detecting chemical, biological, and physical characteristics because of their high sensitivity to variables in the environment.

The objective of this part is to present a thorough overview of PCFs, including information on their different varieties, fabrication processes, guiding mechanisms, essential traits, and wide range of applications. We can recognize the significant influence PCFs have had on

contemporary photonics and their potential for further advancements by comprehending these facets.

## 2.2 Structural Analysis of Photonic Crystal Fibers

Structural analysis of PCFs is crucial for understanding their optical properties and ensuring their performance in various applications. This means examining the properties of the material, fiber geometry, and the placement and dimensions of the air holes.

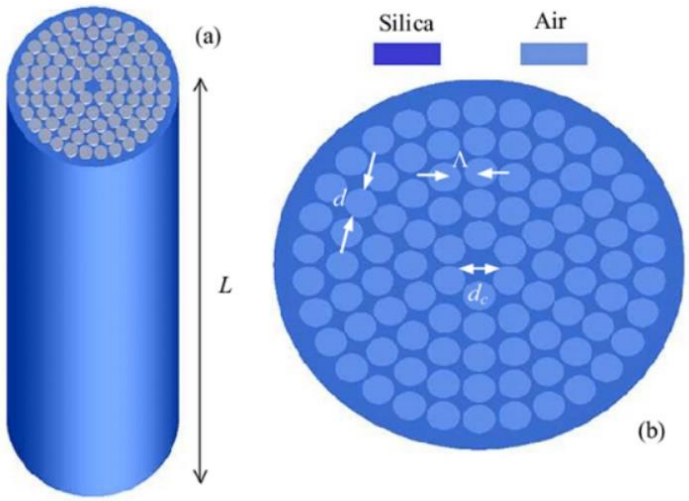


**Figure 2.1:** (a) Cross-sectional view and (b) Longitudinal view of PCF

**Dimensions of Microstructure**

The microstructure geometry of PCFs, which comprises the quantity, orientation, and size of air holes, has a significant impact on the guiding characteristics of the material. Techniques like scanning electron microscopy (SEM) and transmission electron microscopy (TEM) are used to visualize and measure microstructure with high precision. These evaluations help achieve desired optical properties, such as specific nonlinearity and dispersion characteristics, by optimizing the fiber design.

**Composition of the Material**

The contrast, attenuation, and nonlinearity of PCFs' refractive index are all impacted by their material composition. To ascertain the composition and distribution of elements within the fiber, elemental analysis techniques including X-ray photoelectron spectroscopy (XPS) and energy-dispersive X-ray spectroscopy (EDX) are utilized. Achieving excellent performance

requires that the materials used in PCF production be pure and consistent, which is ensured by these analyses.

**Uniformity of Air Holes**

The air holes' uniformity is essential for reliable optical performance. The overall performance of the fiber can be impacted by variations in light propagation caused by changes in the size and geometry of the air holes. Techniques like optical microscopy and interferometry are employed to evaluate the air hole homogeneity over the fiber's length.

**Mechanical Characteristics**

Comprehending the mechanical characteristics of PCFs is crucial for their effective application. This entails assessing the fiber's resilience to external elements like humidity and temperature as well as its tensile strength and flexibility. Mechanical testing, which includes dynamic mechanical analysis (DMA) and tensile testing, gives information about the robustness and endurance of the fibers and makes sure they can survive the circumstances of the applications for which they are designed.

**Profile of Refractive Index**

The optical characteristics and guiding mechanism of a PCF are determined by its refractive index profile. Interferometric techniques and refracted near-field (RNF) profiling are two approaches used to evaluate the distribution of refractive index across the fiber cross-section. To create fibers with particular dispersion and guiding properties, accurate profiling is necessary.

## 2.3 Categories of Photonic Crystal Fibers

Photonic Crystal Fibers (PCFs) can be classified according to their light-guiding systems and structural layout. Understanding their many applications and features is made easier by this classification.

### *2.3.1 Classification of Structural Designs*

- **Solid-Core PCFs:** These PCFs feature a cladding which has a regular pattern of air holes encircling a solid core. Usually, silica or another substance with a high refractive index is used to make the core.

- **Hollow-Core PCFs:** These fibers have a periodic-structured cladding encircling an air- or other low-refractive-index material-filled core. Attenuation is decreased by this design, which limits the contact between light and the fiber material.
- **Multi-Core PCFs:** These fibers have several cores encased in a single cladding structure, each with a unique set of air holes surrounding it. Applications needing low crosstalk and high spatial multiplexing are served by multi-core PCFs.
- **Chalcogenide and Fluoride Glass PCFs**: PCFs made of materials other than silica, such as glasses with chalcogenide or fluoride content, have special optical qualities like longer transmission windows and larger nonlinearities.

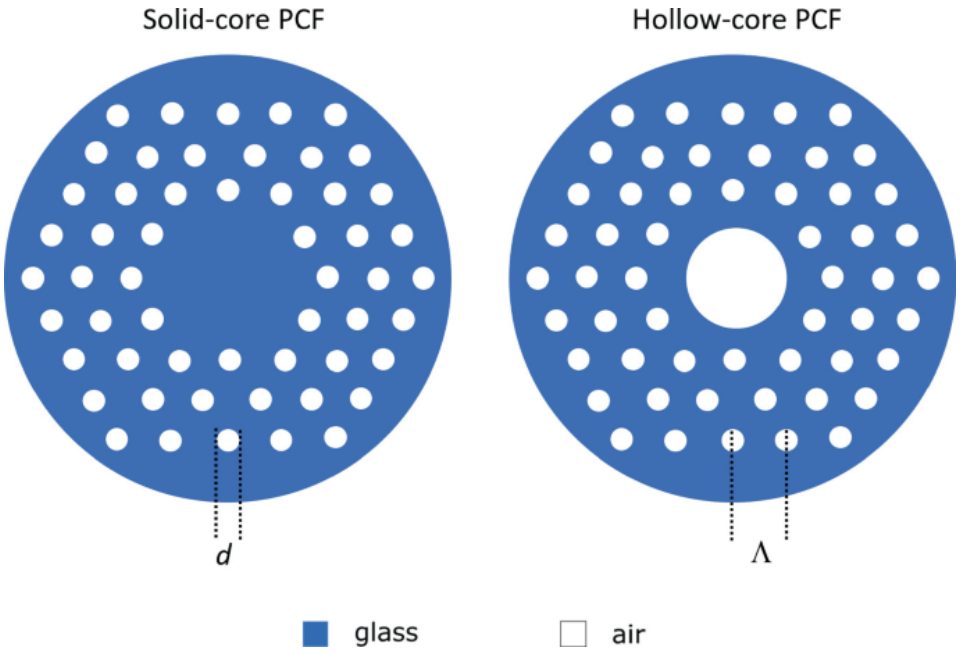


**Figure 2.2:** Solid-core PCF and Hollow-core PCF

### *2.3.2 Classification of Light-Guiding Mechanisms*

- **Index-Guiding PCFs:** As the cladding has a lower effective refractive index compared to the core, light is restricted to the core through modified total internal reflection. Similar to conventional fibers, but with more control over dispersion and nonlinearity, is this kind of PCF.
- **Photonic Bandgap PCFs:** These fibers use a core that has a lower refractive index compared to the cladding to guide light through. The cladding's periodic structure produces a photonic bandgap that limits the propagation of some wavelengths, containing the light inside the core.

- **ARROWs, or Anti-Resonant Reflecting Optical Waveguides**, are PCFs that reflect light at the interface between a low-index cladding and a high-index core. This system works well for steering light across a wide range of wavelengths with limited loss.

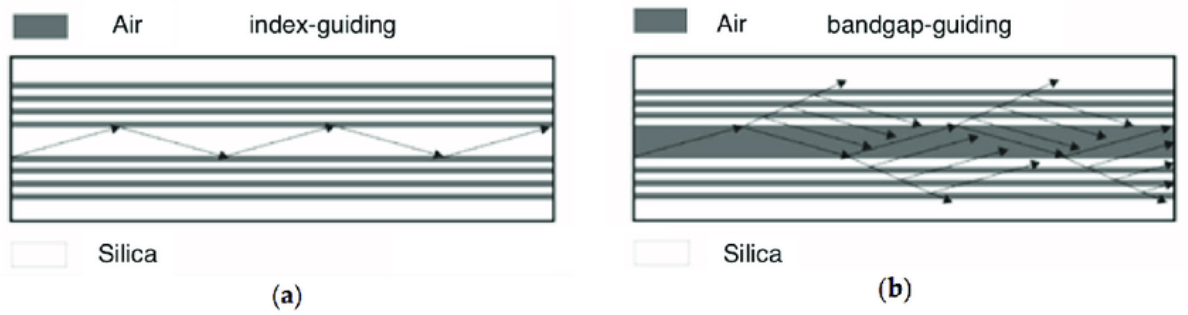


**Figure 2.3:** (a) Index-guiding and (b) Bandgap-guiding PCF

### *2.3.3 Light Guidance Mechanisms*

- **Complete Internal Analysis:** To keep light inside the core, index-guiding PCFs rely on entire internal reflection. Because the air holes of the cladding area have a lower effective refractive index than the core, light can pass through the core entirely through internal reflection.
- **Effect of Photonic Bandgap:** Photonic bandgap photonic crystal fibers direct light using the photonic bandgap phenomenon. The cladding's periodic structure generates a bandgap that confines some wavelengths inside the core by preventing them from propagating. When hollow-core PCFs are used, this technique works especially well for directing light since the cladding has a higher refractive index compared to the core.
- **Resonance-Avoiding Reflection:** Light is guided via anti-resonant reflecting optical waveguides (ARROWs), which reflect light at the interfaces between a low-index cladding and a high-index core. This technique works well for low-loss guiding light over a wide wavelength range and is employed in several hollow-core PCFs.

## 2.4 Key Characteristics

Understanding the distinct optical and structural characteristics of PCFs that determine how well they function in diverse applications is necessary for characterization. Mode structure, dispersion characteristics, nonlinearity, birefringence, attenuation, and confinement loss are important characterizations.

- **Mode Structure**

Depending on their design, PCFs can handle either single-mode or multi-mode operation. For applications like high-precision metrology and telecommunications that demand minimal dispersion and good beam quality, single-mode PCFs are essential. On the other hand, multi-mode PCFs have a greater power capacity and are employed in devices like high-power lasers.

In order to characterize mode structure, one must determine whether the fiber can support a given set of spatial modes of light. Approaches like mode field diameter (MFD) measurements and near-field scanning optical microscopy (NSOM) are frequently used to examine the mode distribution and guarantee single-mode or multi-mode functioning as needed.

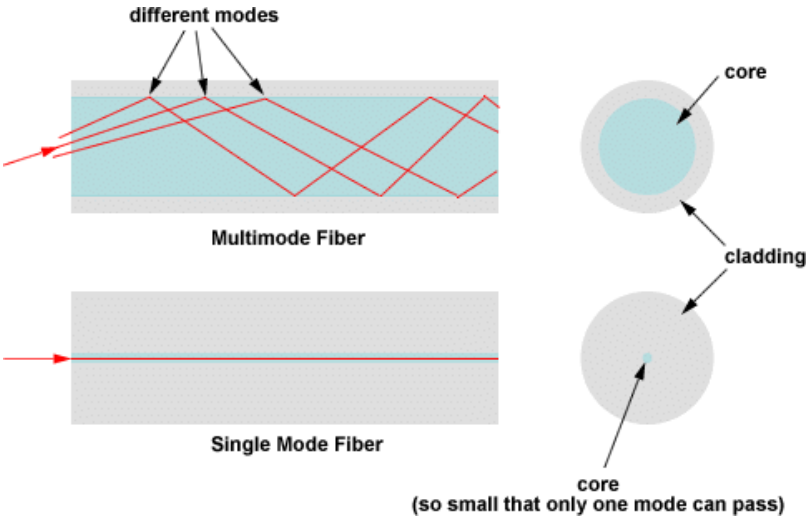


**Figure 2.4:** Multi-mode fiber and single-mode fiber mechanisms

- **Dispersion Characteristics**

The adjustable dispersion characteristics of PCFs are among their biggest benefits. Applications can be customized for the dispersion by altering the size and configuration of the air holes. Among other things, this entails producing fibers that, at specific wavelengths, have zero dispersion—a necessary component for supercontinuum generation and nonlinear optics.

Typically, spectral or white light interferometry is used for dispersion characterisation. Here, various wavelengths are used to measure the dispersion parameters, such as group velocity

dispersion (GVD) and chromatic dispersion. For PCFs to be optimized for applications that need precise control over pulse propagation, these measurements are essential.

- **The Absence of Linearity**

Because of their small core size and high contrast between refractive indices, PCFs show high nonlinearity. This makes them perfect for nonlinear optics applications including frequency conversion, soliton propagation, and supercontinuum creation.

- **Birefringence**

High birefringence, or the variation in refractive indices for various light polarization states, can be exhibited via PCF design. For polarization-maintaining fibers used in applications requiring steady polarization, high birefringence is advantageous.

- **Diminishment**

Cut-back or transmission loss measurements, which compare the input and output power levels over a defined length of fiber, are used to measure attenuation in PCFs.

- **Loss of Confinement**

From the core, the loss of light that seeps into the cladding which is referred to as confinement loss. Numerical simulations utilizing techniques such as the finite element method (FEM) and finite-difference time-domain (FDTD) analysis are necessary to characterize confinement loss.

## 2.5 Why PCF?

PCFs are more suited for sophisticated applications than ordinary optical fibers since they have a number of benefits over them.

- **Increased Flexibility in Design**

PCFs offer more design flexibility than conventional fibers. One can customize the periodic array of air holes to attain particular optical characteristics, such zero dispersion, strong nonlinearity, or distinct guiding mechanisms. Fibers designed for certain applications, such as high-power transmission or supercontinuum generation, can be created thanks to this design flexibility.

- **Adaptable Dispersion Characteristics**

PCFs enable adjustable dispersion characteristics, in contrast to conventional fibers that have set dispersion characteristics. The size and configuration of the air holes allow for exact adjustment of the dispersion to suit the requirements of individual applications. This is critical for nonlinear optics and telecommunications applications, where signal integrity and performance depend on the management of dispersion.

- **Increased Nonlinearity**

In comparison to conventional fibers, PCFs exhibit increased nonlinearity because of their tiny core size and high refractive index contrast. Because of this, PCFs are especially useful in processes like frequency conversion, supercontinuum creation, and soliton propagation that call for strong nonlinear effects. More compact and efficient nonlinear optical devices are made possible by the increased nonlinearity.

- **Better Light Containment**

When it comes to light confinement, PCFs—particularly those that use the photonic bandgap or anti-resonant reflection mechanisms—offer better results than conventional fibers. Because of their ability to reduce losses and increase light propagation efficiency, PCFs are the perfect choice for applications that need long-distance transmission with low attenuation.

- **Flexibility in Material Selection**

A multitude of materials, such as silica, chalcogenide, and fluoride glasses, can be used to create PCFs. Because of their adaptability, fibers with longer transmission windows and special optical characteristics can be developed for a variety of uses, including high-power delivery and infrared transmission.

- **Superior Sensitivity for Sensing-Related Uses**

In sensing applications, high sensitivity is made possible by PCFs' distinct structure. PCFs are perfect because light's interaction with the surroundings can be accurately controlled.

## 2.6 Fabrication Methods

- **Stack-and-Draw Technique**

A popular process for creating PCFs is stacking silica rods and capillary tubes to create the required microstructure, which is subsequently pulled into a fiber. This makes it possible to precisely manipulate the fiber geometry.

- **The process of extrusion**

To produce the required microstructure, glass and air are forced into a mold during the extrusion process. Fibers with intricate cross-sections and large-scale structures can be produced with this technique in especially well.

- **The 3D Printing Process**

3D printing is a cutting-edge technology that makes it possible to fabricate PCFs with complex designs that are challenging to create with conventional techniques. This method allows for a considerable deal of design flexibility and can produce fibers with unique shapes for particular uses.

## 2.7 Uses of PCFs

- **Telecommunications**

Because PCFs can handle high data speeds and low dispersion and attenuation long-distance transmission, they improve optical communication systems.

- **Medical Sensing**

PCFs are perfect for biological sensing applications because of their high sensitivity and customizable characteristics, which allow for early illness diagnosis and monitoring.

- **Environmental Observation**

Due to their great sensitivity and specificity, PCFs are used in environmental monitoring to identify hazardous compounds and tiny levels of contaminants.

- **Industrial Rework**

PCFs are used in industrial processing for accurate measurements and control. They are appropriate for material analysis, process monitoring, and quality control applications.

# Chapter 3

# Exploring SPR and LSPR: Surface Plasmon Resonance and Localized Surface Plasmon Resonance

## 3.1 Introduction of SPR

A highly sensitive and non-invasive optical method that has proven essential for identifying and examining molecule interactions at metal-dielectric interfaces is surface Plasmon Resonance, or SPR. SPR was first applied in basic physics research and has since developed into an essential tool in material science, biology, and environmental monitoring. The method takes use of surface plasmons' resonant oscillations, which are coherent electron oscillations at the metal surface that are extremely responsive to variations in the local refractive index. Because of its sensitivity, SPR is an effective real-time, label-free biomolecular contact detection technique.

SPR is a well-known analytical method used to study interactions between molecules and surfaces as well as the interactivity of biomolecules like proteins, DNA, and RNA [1]. The basis of SPR is the observation of changes in the refractive index close to the metal surface as molecules attach themselves to it [2]–[5]. The novel Surface Plasmon Resonance using Photonic Crystal Fibers technique makes use of optical fibers with regulated air hole designs to improve SPR performance [6]. The study of protein-protein interactions, DNA and RNA connections, biological detection and testing, pharmaceutical science, toxicology, nanoparticle relations, biomedical and biochemical uses and more have all made substantial use of SPR sensors [5].

Applications in terahertz sensors [7]–[11], [optical communications [12], [13], wave transmission [14], blood constituent identification [15], and many other specific domains are also noteworthy.

## 3.2 Working Mechanism of Surface Plasmon Resonance

The interaction of polarized light with a metal-dielectric contact is at the core of the SPR principle. Surface plasmons are excited when polarized light contacts a metal layer at a particular resonance angle, creating a resonance condition that is extremely sensitive to variations in the local refractive index.

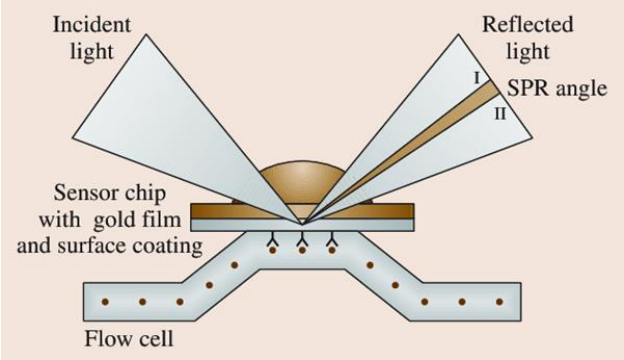


**Figure 3.1:** Presence of Surface Plasmon Resonance by the absorption and reflection of light

At the contact with a dielectric media, polarized light, usually from a laser, is first directed onto a metal film, commonly made of gold or silver. Surface plasmons are excited when incident light energy transfers to the surface electrons at a specific incidence angle called the resonance angle. When the momentum of the incident light and the surface plasmons are equal, a resonance condition arises. Resonance is identified by measuring the intensity of reflected light, which exhibits a steep dip at resonance. Resonance is shifted by any change in refractive index in the vicinity of the metal surface.

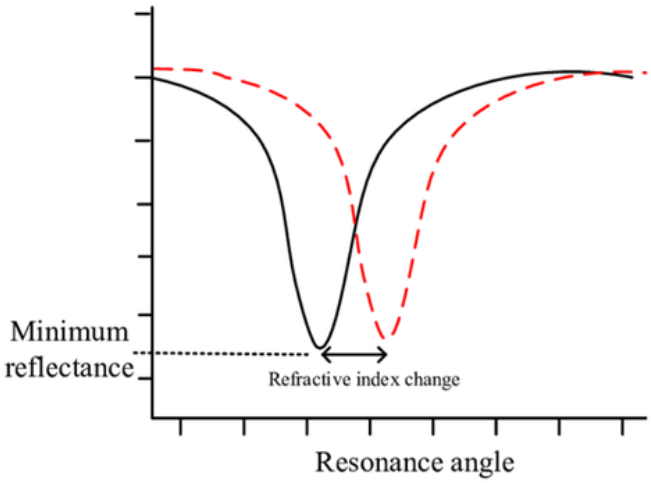


**Figure 3.2:** Creation of Resonance Angle at different refractive index along the metal surface

### *3.2.1 Surface Plasmon Wave (SPW)*

An electromagnetic wave called a Surface Plasmon Wave (SPW) is produced when incident light interacts with the metal electrons at the metal-dielectric contact [16]. SPWs degrade exponentially perpendicular to the surface, and they are limited to the interface. High spatial resolution is made possible by their wavelengths, which are shorter than those of the incident light. For sensing applications, SPWs are perfect because of their high sensitivity to changes in refractive index.

### *3.2.2 Evanescent Field*

When light experiences total internal reflection at the metal-dielectric interface, a near-field phenomena known as the evanescent field is created. It extends into the dielectric medium next to the metal surface and, as one moves away from the interface, decays exponentially. Since the evanescent field interacts with molecules close to the metal surface, it is essential to SPR sensing. The sensing range is restricted to the local area of the metal surface due to the decay length, which is typically on the scale of hundreds of nanometers. This field's molecules change the local refractive index, which modifies the SPR signal and makes it necessary to detect target analytes.

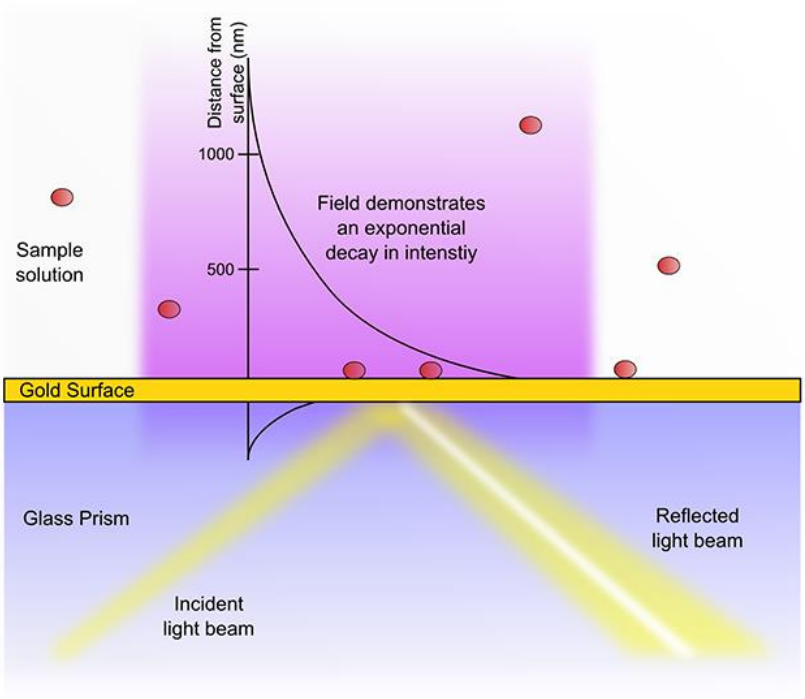


**Figure 3.3:** Visualization of Evanescent Wave

### *3.2.3 Confinement Loss*

The energy lost during the surface plasmon wave's propagation along the metal-dielectric contact is referred to as confinement loss in surface plasmon resonance (SPR). The primary causes of this loss are light absorption by the metal and surface roughness-induced dispersion. The choice of metal, usually silver or gold, affects confinement loss because of variations in its absorption properties. The metal's surface defects can shorten the surface plasmon wave's propagation length by increasing scattering losses. Furthermore, confinement losses are typically larger at shorter wavelengths, which reduces the SPWs' effective propagation distance.

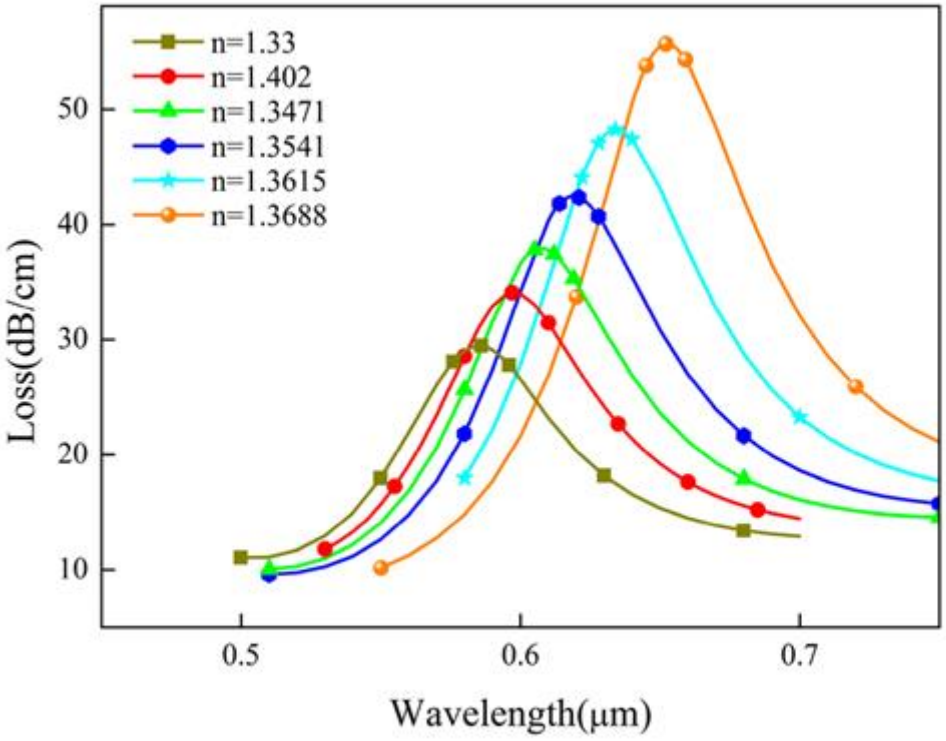


**Figure 3.4:** Different amount of confinement loss from different resonance lengths

## 3.3 Why SPR?

SPR is used in many applications because to its numerous noteworthy advantages over conventional optical sensing approaches. Low analyte concentrations can be found thanks to the technique's ability to detect minute changes in refractive index. SPR does not require tagging of the analytes, in contrast to fluorescence-based approaches, which preserves the analytes in their natural state and streamlines the detection process. Moreover, SPR offers real-

time information on molecular interactions, making kinetic analysis and dynamic studies of binding events possible. Because of its great sensitivity and wide range of applications, it is useful in numerous fields such as chemical analysis, environmental monitoring, and biosensing.

### *3.3.1 Benefits of SPR*

- **High Sensitivity:** SPR has the ability to identify even the smallest variations in refractive index, making it possible to identify analyte concentrations as low as possible.
- **Label-Free Detection:** SPR eliminates the need for analyte labeling, streamlining preparation and maintaining the molecules' original state.
- **Real-Time Monitoring:** The method offers data on molecular interactions in real-time, which is essential for researching binding kinetics and events.
- **Broad Applicability:** SPR has applications in material science, biosensing, and environmental monitoring, among other domains.
- **Dynamic Range:** SPR is capable of detecting analyte concentrations ranging from extremely low to comparatively high.
- **Versatility**: A wide range of sample types, such as liquids, gases, and thin films, can be used with this approach.

## 3.4 Implementation of SPR

SPR implementation requires a number of essential elements and exact procedures to provide precise and trustworthy measurements.

### *3.4.1 Parts*

- **Light Source:** The incident light required to generate surface plasmons is produced by a polarized laser.
- **Metal Film:** A coating of gold or silver applied to an optical fiber or glass prism.
- **Prism Coupler:** Enables light to be coupled into the metal film at the proper angle.
- **Detector:** Tracks changes in the resonance angle by measuring the intensity of the reflected light.

### *3.4.2 Procedure for Implementing SPR*

- **Metal film** preparation involves applying a thin layer of metal to an appropriate substrate, such as an optical fiber or glass prism.
- **Light Source Alignment**: The polarized laser is positioned so that it strikes the metal-dielectric interaction at the right angle.
- **Sample Introduction:** In the dielectric medium next to the metal surface, the analyte sample is added.
- **Measurement and Analysis:** Shifts in the resonance angle, which signal variations in the local refractive index, are identified by tracking variations in the intensity of reflected light.

## 3.5 SPR's limitations

SPR is an effective strategy, but it has a few drawbacks that need to be taken into account.

### *3.5.1 Principal Limitations of SPR*

- **Limited Penetration Depth:** Only the immediate region of the metal surface is probed by the evanescent field, which keeps the sensing depth to a few hundred nanometers.
- **Constraints on Metal Selection:** Although gold and silver are frequently used metals, their unique optical qualities and chemical stability may make them unsuitable for some applications.
- **Environmental Sensitivity:** SPR measurements need to be carefully controlled and calibrated because they might be impacted by environmental factors like temperature variations.
- **Cost & Complexity:** Accurate measurements necessitate perfect alignment and high-quality equipment, which might raise the cost and complexity of SPR setups.
- **Non-Specific Binding:** In order to reduce false positives caused by non-specific binding of molecules to the sensor surface, surface chemistry techniques must be applied with effectiveness.

## 3.6 Introduction of LSPR

Excitation of metallic nanoparticles by light causes the collective oscillations of conduction electrons to produce the potent optical phenomena known as Localized Surface Plasmon Resonance, or LSPR. This resonance is particularly sensitive to the local refractive index around the nanoparticles and happens at specific wavelengths. Because of its remarkable sensitivity and capacity to deliver comprehensive information about molecular interactions at the nanoscale, LSPR has found many applications in material science, nanophotonics, and chemical and biological sensing.

## 3.7 Working Mechanism of Localized Surface Plasmon Resonance

Light-metal nanoparticle interaction is the basis for the LSPR mechanism of operation. The conduction electrons at the surface of these nanoparticles oscillate collectively in response to light [17], [18]. The localized surface plasmon, which is caused by this oscillation, is a localized increase of the electromagnetic field surrounding the nanoparticle.

When the incident light frequency and the natural frequency of the electron oscillations coincide, the resonance condition is reached. The size, form, and makeup of the nanoparticles as well as the surrounding dielectric environment all have a significant impact on this resonance. Sensitive molecular contact detection is made possible by shifts in the resonance wavelength caused by changes in the local refractive index, such as molecular binding to the surface of nanoparticles.

### *3.7.1 Surface Plasmon Wave (SPW)*

By limiting the surface plasmon wave to the area around the nanoparticle, LSPR produces an increased electromagnetic field that is referred to as a "hot spot." Because of these hot spots' extreme sensitivity to variations in the local refractive index, LSPR is a useful technique for identifying molecule interactions at extremely low concentrations.

LSPR uses non-propagating, confined oscillations around the nanoparticle as opposed to SPR, which includes propagating surface plasmon waves along a metal-dielectric contact. Due to

this localization, the nanoparticle is more sensitive to its near surroundings and experiences a significantly stronger field enhancement.

### *3.7.2 Evanescent Field*

The near-field area surrounding the nanoparticle where the electromagnetic field is noticeably amplified is referred to as the evanescent field in LSPR. This field normally extends a few nanometers into the surrounding medium before decaying exponentially from the nanoparticle surface.

The local refractive index shifts the LSPR peak due to interactions between molecules at the nanoparticle surface and the amplified evanescent field. For sensing applications involving small volumes or surface-bound analytes, LSPR is especially useful because of the great confinement of the evanescent field to the nanoparticle surface.

### *3.7.3 Confinement Loss*

In LSPR, the term "confinement loss" describes the energy lost during the oscillation of the localized surface plasmon. The metal's intrinsic absorption and the nanoparticle's scattering are to blame for this loss. The kind of metal, the size, shape, and wavelength of the incident light are some of the variables that affect the degree of confinement loss.

Because of their advantageous plasmonic characteristics, such as reduced confinement losses in comparison to other metals, metals like gold and silver are frequently employed in LSPR. Similar to SPR, surface flaws and roughness can raise scattering losses, which can impair the sensor's overall performance and sensitivity.

## 3.8 Why LSPR Over SPR

Compared to conventional optical sensing methods and, in some cases, even SPR, LSPR has a number of important advantages [19]:

- **High Sensitivity:** LSPR can identify incredibly minute variations in the local refractive index, making it possible to identify analyte concentrations as low as possible.

- **Nanometer-Scale Sensing:** LSPR's confined structure offers remarkable spatial resolution, which makes it perfect for investigating single-molecule detection and nanoscale interactions.

- **Versatility:** A broad range of nanoparticle sizes, shapes, and compositions can be used with LSPR, allowing customisation for particular applications.

- **Robustness:** Compared to SPR, LSPR-based sensors are usually more resistant to changes in the environment, which makes them appropriate for a wide range of real-world applications.

- **Broad Applicability**: The method can be used in a variety of domains, such as material science, biosensing, medical diagnostics, and environmental monitoring.

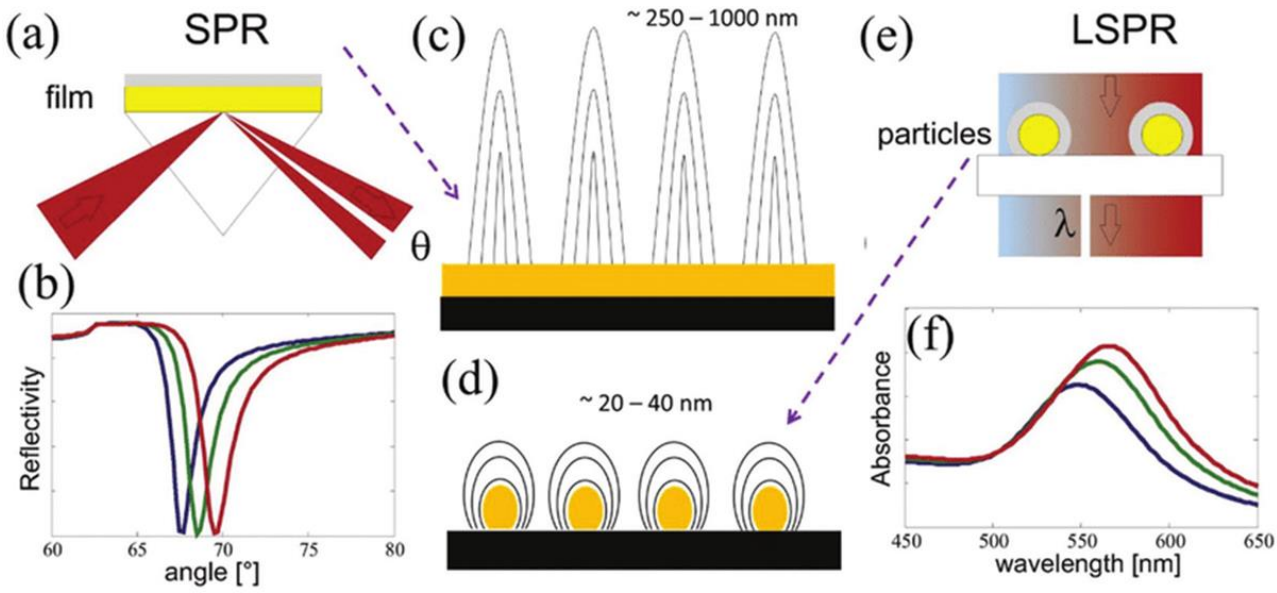


**Figure 3.5:** A side by side view of (a) SPR and (b) LSPR

Furthermore, SPR sensors have poor mechanical durability due to their thick cladding layers, and their production procedures are more complex [20].

## 3.9 Implementation of LSPR

To guarantee precise and dependable measurements, LSPR implementation requires a number of essential parts and procedures. First, controlled-size and -shaped metallic nanoparticles, usually made of silver or gold, are synthesized. After that, these nanoparticles are either suspended in a solution or immobilized on an appropriate substrate.

The nanoparticles are illuminated by a light source, often a laser or a broadband light source. With the use of a spectrometer to analyze the absorption or scattering spectra, the interaction between light and the nanoparticles is observed. The local refractive index and chemical interactions can be inferred from the LSPR peak position and intensity.

### *3.9.1 Procedure for Implementing LSPR*

- **Synthesis of Nanoparticles:** To obtain the required plasmonic properties, metallic nanoparticles are manufactured with exact control over their size, shape, and composition.

- **Surface Functionalization:** To improve the selectivity of the nanoparticles for the target analytes, they are functionalized with certain compounds or coatings.

- **Sample Introduction:** Usually in the form of a thin layer on the substrate or in a solution, the analyte sample is delivered in close proximity to the nanoparticles.

- **Optical Measurement:** Changes in the LSPR peak are identified by employing absorption or scattering spectroscopy to quantify the light-nanoparticle interaction.

## 3.10 LSPR's Limitations

Although LSPR is an effective method, there are a few drawbacks that need to be taken into account:

- **Limited Penetration Depth:** LSPR's utility for identifying bulk characteristics is limited because its sensing range is only a few nanometers surrounding the nanoparticle.

- **Environmental Factor Sensitivity:** The LSPR signal is sensitive to changes in temperature, pH, and other environmental conditions, necessitating careful control and calibration.

- **Nanoparticle Stability:** The repeatability and dependability of LSPR measurements can be impacted by the stability of nanoparticles, notably their propensity to agglomerate.

- **Difficulties in Surface Functionalization:** Selective binding of target analytes can be achieved through the effective functionalization of nanoparticles, which can be complicated and need careful tuning.

- **Non-Specific Binding:** When molecules bind non-specifically to the surface of nanoparticles, it might produce false positives, which calls for efficient surface chemistry techniques.

# Chapter 4

# Sensing Mechanisms and Plasmonic Materials

## 4.1 Introduction

One essential optical method for detecting molecule interactions at metal-dielectric surfaces is surface Plasmon Resonance (SPR). SPR has been implemented in a variety of ways, each having unique applications and methods. The main SPR techniques are examined in this section, with a particular emphasis on prism-based techniques and the distinctions between internal and exterior sensing sensors. Also, plasmonic materials are discussed.

## 4.2 Prism-Based Approach and Mechanism

The prism-based approach, particularly the Kretschmann configuration, is the most widely used method for exciting surface plasmons. This technique involves the use of a prism to couple light into a metal film at a specific angle, achieving the necessary conditions for SPR.

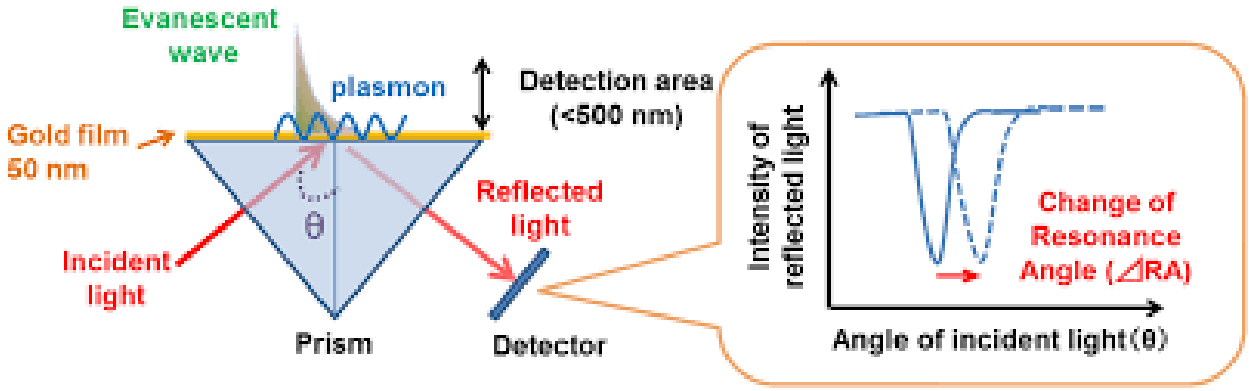


**Figure 4.1:** Prism based SPR sensor

In this arrangement, the base of a prism covered in a thin layer of metal, usually silver or gold, is illuminated by a monochromatic light source, usually a laser. At the metal-dielectric interaction, all of the light is internally reflected. The incident light's wave vector coincides with the surface plasmons at a specific angle called the resonance angle. An evanescent wave that pierces the dielectric medium just a short distance is produced by this resonance situation, which permits energy transfer from the light to the surface plasmons. Surface plasmon excitation is indicated by a dip at the resonance angle in the reflected light intensity, which is

monitored. The detection of molecular interactions is made possible by this dip, which shifts in response to changes in the refractive index close to the metal surface.

### *4.2.1 Difficulties in Prism-Based Approach*

The prism-based technique is effective, but it has a few drawbacks. The arrangement is frequently large and necessitates exact alignment, which restricts its portability and integration into small devices. It might be difficult to achieve the right angle for surface plasmon excitation and total internal reflection, necessitating exact control. The resonance condition can be impacted by changes in ambient factors like pressure and temperature, hence precise calibration is required. Plasmon resonance can be interfered with by surface roughness and pollution, which lowers sensitivity and accuracy. In addition, some applications may be limited by the requirement that the sample be in close proximity to the metal film, particularly in complex sample settings.

## 4.3 Internal Sensing Sensors

For sensing purposes, internal sensing sensors make use of the evanescent field produced at the metal-dielectric interface. These sensors frequently employ an optical fiber or waveguide arrangement, with the metal film placed on the waveguide's surface. Analyte molecules can directly interact with the evanescent field created at the metal-dielectric interface by light traveling through the waveguide, changing the local refractive index. When the light's wave vector coincides with that of the surface plasmons, a discernible shift in the intensity of the reflected or transmitted light occurs, fulfilling the resonance condition.

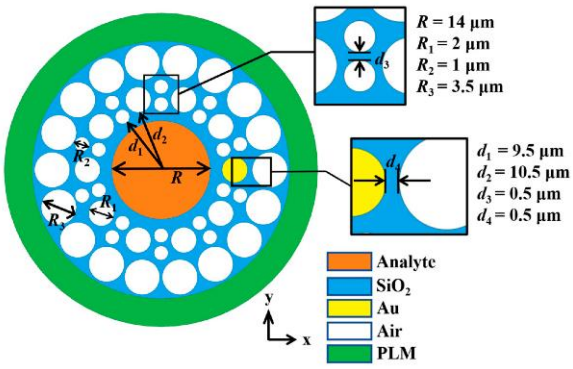


**Figure 4.2:** A PCF sensor based on internal sensing approach

Compactness and the analyte's near proximity to the metal film, which guarantees a strong interaction with the evanescent field and improves sensitivity, are two benefits of internal sensing sensors. However, their sensitivity is restricted by the confined sensing volume of the evanescent field zone and requires a clean metal surface to be maintained.

## 4.4 External Sensing Sensors

The evanescent field that extends outside the waveguide or fiber is interacted with by an external medium in external sensing sensors. These sensors work well in a variety of settings and offer more flexibility when handling samples. The light traveling through a metal-coated waveguide or fiber creates an evanescent field that reaches into an external medium containing the analyte. By observing the reflected or transmitted light, one can determine changes in the resonance condition caused by variations in the refractive index of this medium.

External sensing sensors are appropriate for applications such as flow-through systems because they provide more flexibility in sample introduction and processing. They can be applied in a variety of settings, such as gas and liquid phases. However, it can be difficult to build these sensors in a way that ensures the evanescent field and the external medium interact well, and performance can be impacted by changes in pressure and temperature in the environment.

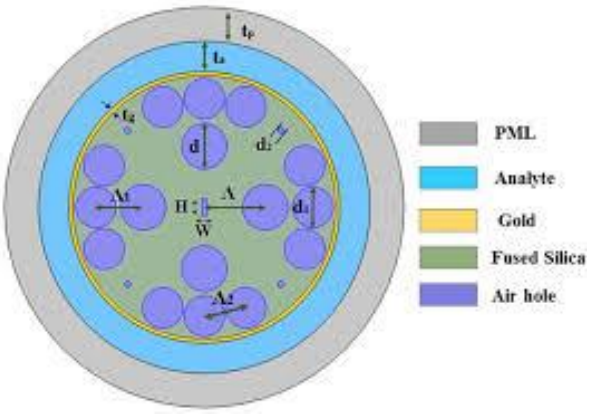


**Figure 4.3:** A PCF sensor based on external sensing approach

Various SPR techniques, such as the more compact internal and exterior sensing sensors and the more conventional prism-based technique, each have their own advantages and difficulties. Comprehending these techniques facilitates the enhancement of SPR-based sensors for diverse uses, ranging from environmental monitoring to the investigation of biomolecular interactions.

The method of choice is determined by the particulars of the application, such as sample handling, sensitivity, and environmental factors.

## 4.5 Why PCF for SPR?

Because of their highly adjustable architectures and superior light confinement, Photonic Crystal Fibers (PCFs) are chosen for SPR over typical optical fibers and prism-based systems.

**Table 4.1:** Comparison between Prism based, Optical fiber based and PCF based SPR sensors

| **Feature** | **Prism** | **Optical Fiber** | **Photonic Crystal Fiber (PCF)** |
|---|---|---|---|
| Structure | Bulk, solid material | Hollow, cylindrical structure | Hollow, cylindrical structure with regularly arranged voids |
| Waveguide type | Diffractive | Graded-index | Photonic crystal |
| Bending loss | High | Low | Very low |
| Attenuation | Moderate (0.1-1 dB/km) | Very low (0.2-0.5 dB/km) | Extremely low (0.01-0.2 dB/km) |
| Dispersion | Can be high or low depending on material and design | Typically low dispersion | Can be engineered for specific dispersion characteristics |

PCFs are adaptable for a range of sensing applications due to their broad wavelength operating and configurable geometries that are made possible by their flexible design. Furthermore,

compared to large prism configurations, PCFs are more portable and easily integrated into gadgets. Additionally, they offer increased mechanical flexibility and resilience to the environment, which makes alignment easier and increases stability in real-world circumstances.

## 4.6 Introduction to Plasmonic Materials

Surface plasmon resonances (SPRs) are coherent oscillations of free electrons at the interface between a metal and a dielectric; materials that can sustain SPRs are known as plasmonic materials. These materials are particularly suited for a variety of sensing applications, such as surface plasmon resonance (SPR) and localized surface plasmon resonance (LSPR) sensors, since they display distinctive optical features like increased electromagnetic fields at particular wavelengths.

### *4.6.1 Infusion of Plasmonic Materials in PCF-SPR Sensors*

Plasmonic materials are usually included into the fiber structure of photonic crystal fiber (PCF)-SPR sensors in order to enable SPR excitation and improve sensor performance. Typically, the infusion procedure entails:

- **Coating the Fiber Core or Cladding:** A thin layer of plasmonic material is applied to the inner surface of the PCF, either the core or the cladding.

- **Techniques for Layer Deposition:** The plasmonic layer is applied uniformly and precisely using techniques such chemical vapor deposition, evaporation, and sputtering.

- **Enhancing Thickness and Uniformity:** Reaching the appropriate resonance and sensitivity requires a certain level of plasmonic layer thickness. Performance consistency is ensured via uniform deposition.

- **Functionalization for Particular Applications:** Chemical or biological agents can be used to further functionalize the plasmonic surface in order to target particular analytes and increase the sensor's specificity and selectivity.

### *4.6.2 Commonly Used Plasmonic Materials for Biosensors*

PCF-SPR sensors frequently employ a variety of plasmonic materials, each with pros and cons.

- Strong and distinct SPR signals in the visible to near-infrared spectrum can be produced by gold (Au), which is extremely robust and oxidation-resistant. It is the best option for biosensing applications because to its biocompatibility. However, the cost of gold and its comparatively significant losses in the infrared limit its usefulness in several applications.

- Compared to gold, silver (Ag) has a stronger SPR signal and greater sensitivity; it works well in the visible and near-infrared spectrums. In contrast to gold, silver is less biocompatible and more prone to oxidation and tarnishing, which might eventually reduce performance.

- Compared to gold and silver, aluminum (Al) is less expensive and more effective in the ultraviolet spectrum. Its performance is lower in the visible and near-infrared spectrums, and because of its oxidation susceptibility, protective coatings are necessary.

- In the visible spectrum, copper (Cu) exhibits plasmonic characteristics akin to those of gold and silver, but it is less costly than gold. However, because of its lower biocompatibility, copper has limited use in biological applications and is very vulnerable to oxidation, which can lead to performance loss.

- Graphene is a relatively new plasmonic material with strong light-matter interaction that enhances sensitivity. It also has a high surface area and variable electrical characteristics. Its integration and fabrication processes are intricate, though, and stability and repeatability issues can arise.

## 4.7 Advent of Metamaterials

Artificially created materials with qualities not seen in naturally existing materials are called metamaterials. They have created new opportunities in the fields of plasmonics and SPR-based sensing because of their extraordinary capacity to control electromagnetic waves.

Typically, metamaterials consist of structures, either periodic or non-periodic, that are smaller than the incident light's wavelength. The performance of SPR sensors can be greatly improved by designing these structures to induce negative refractive indices, superlensing, and cloaking effects.

**Table 4.2:** Overview of Metamaterials vs Conventional Plasmonic Materials

| **Feature** | **Metamaterials** | **Conventional Plasmonic Materials (Silver/Gold)** |
|---|---|---|
| Structure | Artificial structures engineered to exhibit unusual optical properties | Natural materials with unique optical properties |
| Wavelength range | Broader range of tunable frequencies | Limited to visible and near-infrared |
| Losses | Generally lower losses, leading to improved device performance | Higher losses, limiting applications |
| Flexibility | Can be designed to achieve a wide variety of optical properties | Properties are more limited |
| Integration | Can be integrated with other materials and devices | Integration can be challenging due to material properties |
| Cost | Generally, more expensive to fabricate | Less expensive to fabricate |
| Applications | Tunable metamaterials can be used for a wide range of applications, including optical sensing, imaging, and communication | Conventional plasmonic materials are used in a variety of applications, including surface-enhanced Raman spectroscopy (SERS), light-emitting diodes (LEDs), and solar cells |

The use of metamaterials in plasmonics has produced advancements in fields like:

- **Enhanced Sensitivity:** By modifying the interaction between light and matter at the nanoscale, metamaterials can be engineered to increase the sensitivity of plasmonic sensors.

- **Chiral Plasmonics:** The development of chiral plasmonic structures is made possible by metamaterials, which opens up new possibilities for the manipulation of circularly polarized light and advances fields such as optical communication and sensing.

- **Greater plasmonic resonance tunability** is provided by metamaterials, which enables dynamic control of the interaction between matter and light.

- **Negative Refractive Index:** Metamaterials with a negative refractive index can have unusual optical characteristics that help scientists create superlenses and other cutting-edge technologies.

Research on the use of metamaterials in plasmonics is still ongoing, with attempts being made to find new uses and designs for these engineered materials.

### *4.7.1 Metamaterials in SPR Sensing*

A number of sophisticated metamaterials have drawn interest in SPR sensing because of their special qualities and ability to improve sensor performance. Prominent instances consist of:

- Zinc oxide doped with aluminum (AZO) is a transparent conducting oxide that exhibits exceptional plasmonic characteristics in the near-infrared spectrum. It is appropriate for many sensing applications due to its strong chemical stability and comparatively low cost. Its visual performance is, however, not as strong as that of conventional plasmonic materials, such as silver or gold.

- Another transparent conducting oxide that is comparable to AZO but with somewhat different optical characteristics is gallium-doped zinc oxide (GZO). Strong plasmonic resonance and great carrier mobility offered by GZO improve SPR sensor sensitivity. By varying the doping levels, its performance can be tailored to suit a variety of applications.

- A popular plasmonic material with outstanding conductivity and transparency in the visible range is indium tin oxide (ITO). ITO may have its plasmonic characteristics adjusted, and it works well with several types of deposition methods. However, the expense and availability of indium could be disadvantages for large-scale uses.

## 4.8 Factors to Consider While Choosing a Plasmonic Material for Designing Real-Life Sensors

When choosing a plasmonic material for real-world sensor design, there are a number of important considerations to make.

The material must have a strong SPR signal and a high degree of sensitivity to variations in the refractive index of the surrounding medium. The resonance wavelength of the plasmonic material must satisfy the requirements of the application, whether it is in the ultraviolet, near-infrared, or visible spectrum, thus the operational wavelength range is also very important.

In order to guarantee the material's resistance to oxidation and chemical degradation and to sustain its long-term stability and performance, chemical stability is crucial. For biosensing applications, biocompatibility—the ability of a substance to be both non-toxic and compatible with biological samples—is crucial.

The material's availability and cost are important considerations, especially for commercial applications and large-scale production. The material should be easily integrated into sensor designs and compatible with current fabrication techniques, with a controllable level of fabrication complexity.

Lastly, to guarantee the longevity of the selected plasmonic material, the sensor's operational environment—which includes temperature, humidity, and exposure to harsh chemicals—must be taken into account. Through a meticulous assessment of these variables, scientists may determine which plasmonic material best suits the needs of PCF-SPR sensors in order to maximize their effectiveness, dependability, and practicality.

# Chapter 5

# Overview of Research on PCF-SPR Sensors

To improve sensing applications and broaden the range of measurable values, numerous researchers have investigated a variety of irregularly shaped PCF sensors in addition to traditional PCF structures [14], [21]–[24]. This exploration has resulted in the creation of more sophisticated technologies.

Using gold as the plasmonic material, Hasan et al. demonstrated a spiral-like SPR-PCF sensor featuring three rings and six arms that has birefringence asymmetry. This sensor showed an amplitude sensitivity (AS) of 420.4 $RIU^{-1}$ and a wavelength sensitivity (WS) of 4600 nm/RIU [25].

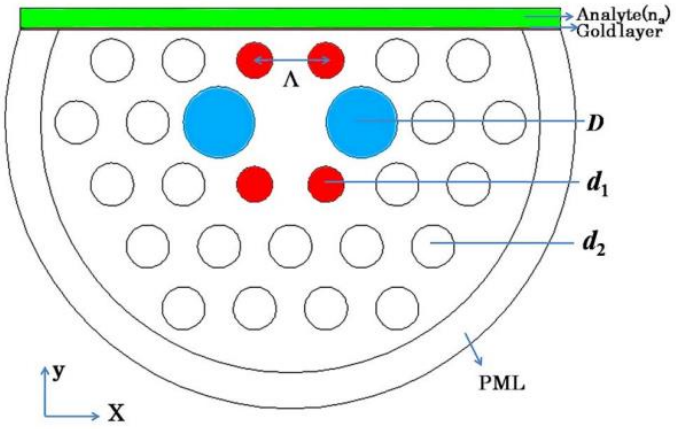


(a)

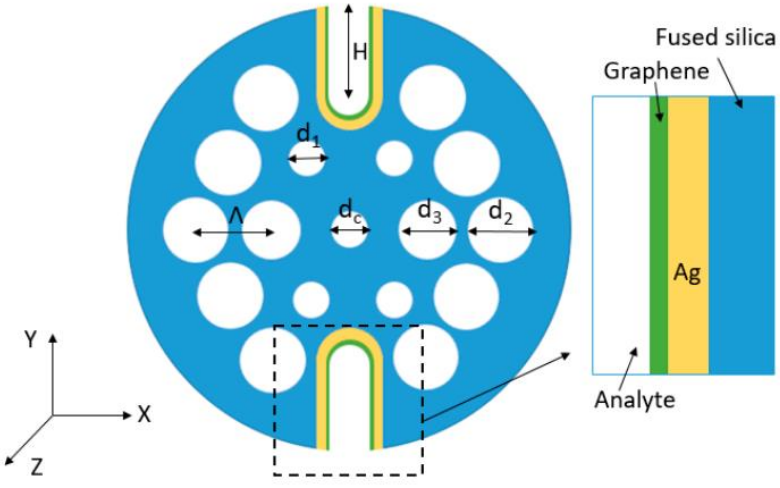


(b)

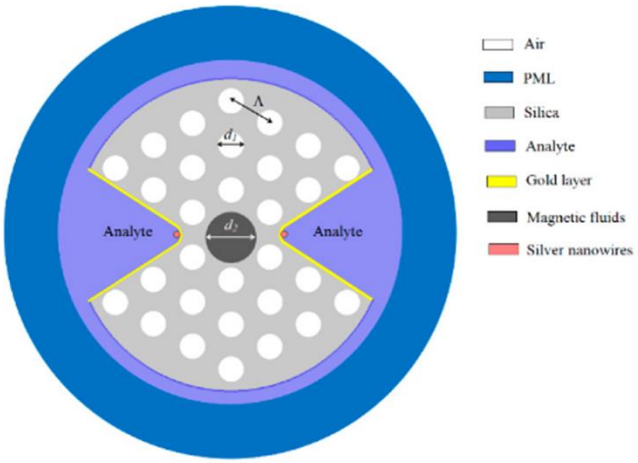


(c)

**Figure 5.1:** Examples of some irregularly shaped PCF sensors (cladding shape)

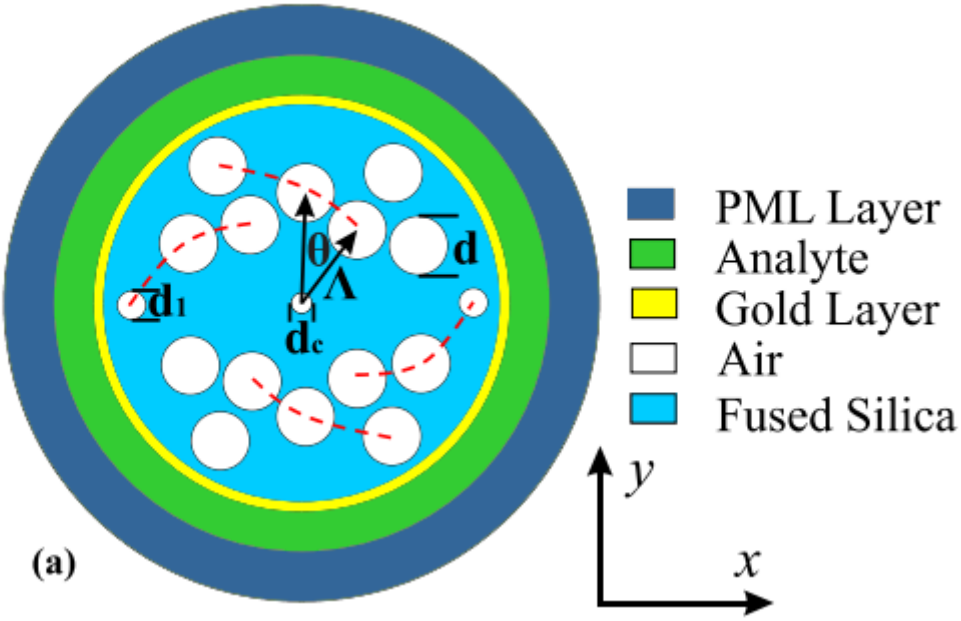


**Figure 5.2:** Spiral-like PCF sensor

A unique PCF sensor that can sense variations in both ambient temperature and magnetic fields was created by Jingwei Lv et al. Their sensor incorporates two silver nanowires along a fan-shaped aperture and uses a dual-channel PCF construction with flat ends coated in gold sheets. In the 1.47–1.52 refractive index region, this design yields a high resolution of $3.22\times10^{-6}$ RIU and a high sensitivity of 31,000 nm/RIU [26].

Xiao et al. developed a sensor that consists of an array of gold (Au) nanowires deposited on a TiO2 layer. This sensor is capable of detecting analytes within a broad refractive index range of 1.08 to 1.37, corresponding to wavelengths ranging from 1210 nm to 2140 nm [27].

Apart from structural modifications, scientists have also investigated the integration of two plasmonic materials in a single sensor. The main purposes of adding TiO2/Graphene films over Gold/Silver-based sensors are to provide strong adhesion and oxidation resistance [28]–[31] TiO2/Graphene-Au/Ag is one example of a bilayer structure that helps improve sensing parameters. A multi-core flat fiber with an amplitude sensitivity (AS) of 820 $RIU^{-1}$ and a sensitivity of 23,000 nm/RIU was created by Rifat et al. using a $TiO_2$ and Au bilayer [29].

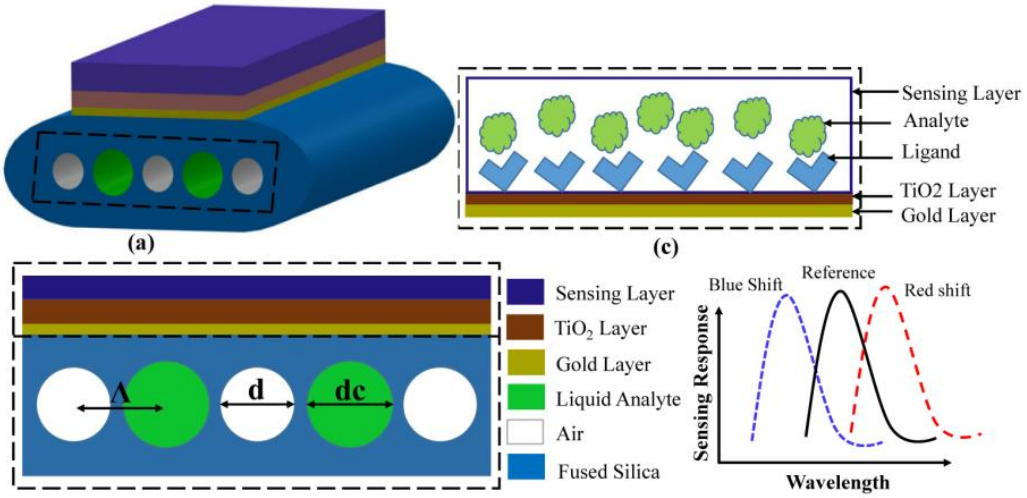


(a)

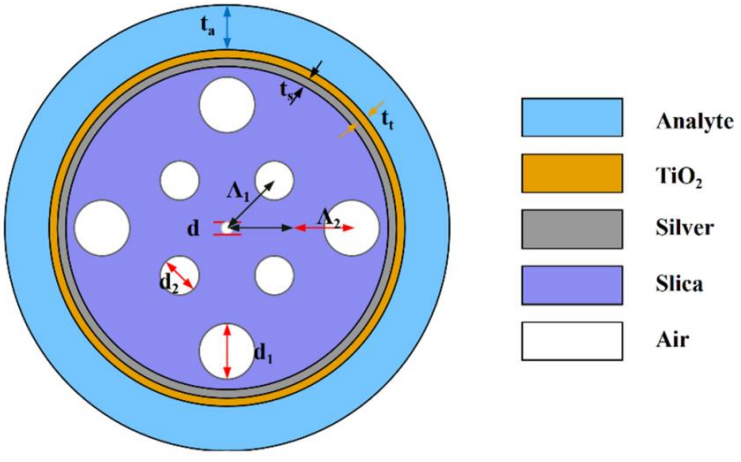


(b)

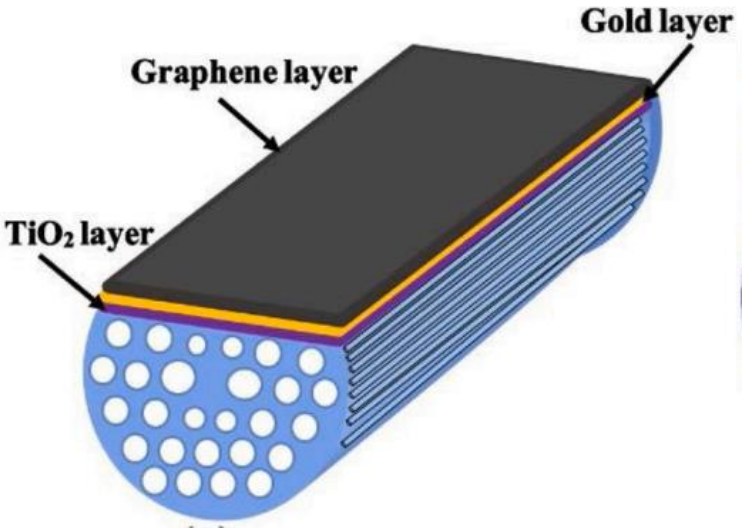


(c)

**Figure 5.3:** Sensor designs incorporating two plasmonic materials

With a combination of TiO2-Au-Graphene, Singh et al. created a sensor design that produced remarkable results, ranging from 48,900 nm/RIU in the refractive index range of 1.32-1.40. Additionally, the sensor showed a figure of merit (FOM) of 611.25 $RIU^{-1}$ and an amplitude sensitivity (AS) of 738.74 $RIU^{-1}$ [31]. Using the phenomena of dual-resonance, further research has also investigated the independent integration of several plasmonic materials into a single sensor [32]–[35].

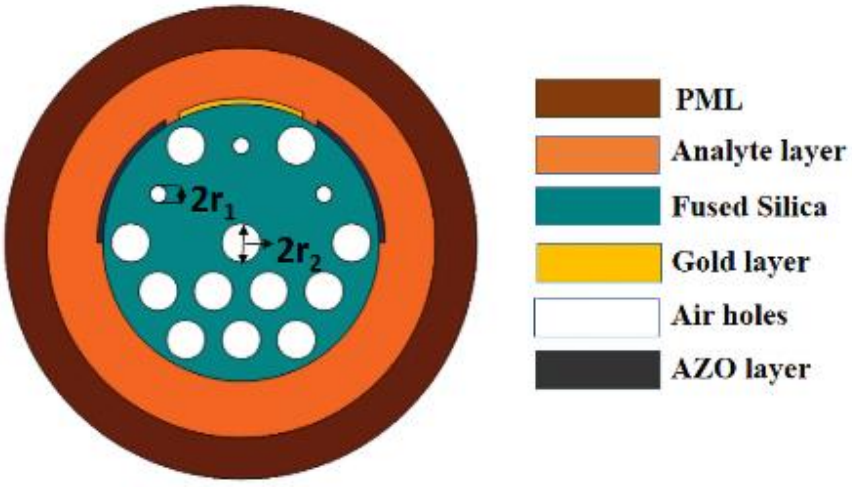


(a)

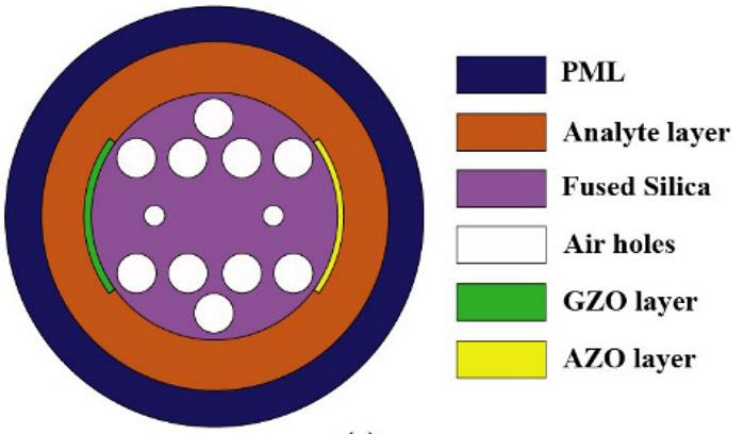


(b)

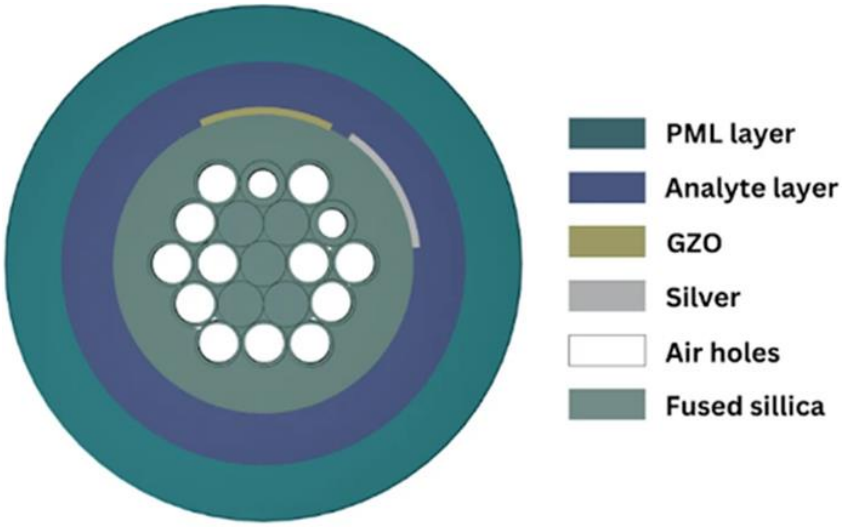


(c)

**Figure 5.4:** Sensor designs incorporating dual-resonance

Sensors have used Au/Ag and Transparent Conductive Oxides (TCO) in conjunction to lower costs and simplify the production process. These materials are selected because of their high doping density and broad bandgap, which allow them to display optical properties in the near-infrared (NIR) region that are comparable to those of metals [36].

# Chapter 6

# Proposed Design: A Novel Wheel-Like Open Core PCF Sensor for Sensing Double Peaks

## 6.1 Introduction

In order to address the difficulties with sophisticated multi-air hole PCFs, this study suggests a simple sensor design that is in line with technological viability for simpler manufacture. Our suggested PCF sensor, in contrast to complex solutions, has an easy-to-produce wheel-shaped structure with three air holes placed 120° apart. The linearity and sensitivity properties of the sensor show promise. The following parts contain comprehensive design requirements, theoretical calculations, fabrication procedures, and comments of the findings.

## 6.2 Sensor Structure and Specifications

In order to address the difficulties with sophisticated multi-air hole PCFs, this study suggests a simple sensor design that is in line with technological viability for simpler manufacture. Our suggested PCF sensor, in contrast to complex solutions, has an easy-to-produce wheel-shaped structure with three air holes placed 120° apart.

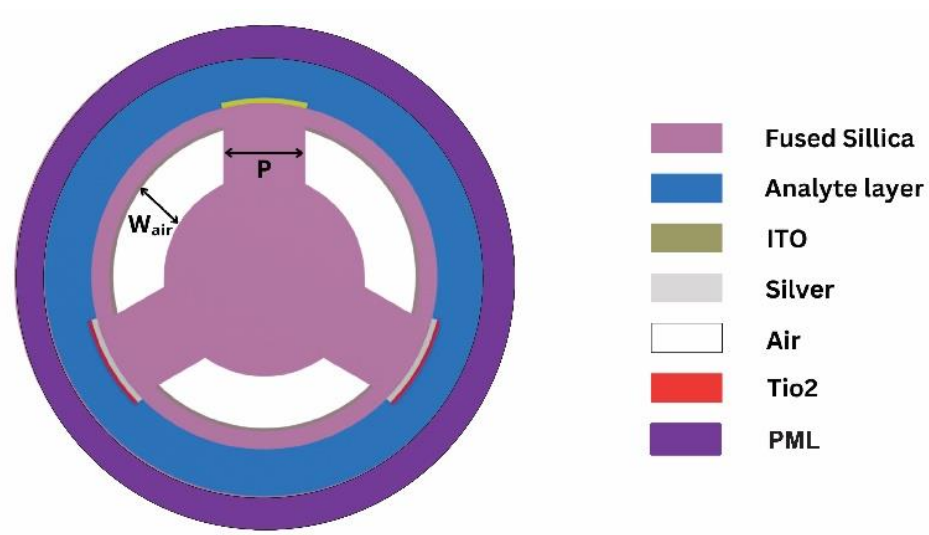


**Figure 6.1:** Architecture of our proposed sensor

## 6.3 Materials Used for the Sensor

A bimetallic layer consisting of titanium dioxide and silver is put on the sidewalls, and a layer of ITO (10 wt%) is applied on top. ITO is very helpful because of its high carrier concentrations, low infrared loss, and adjustable photoelectric characteristics [37]. Using an ITO-based D-shaped PCF sensor, previous studies have shown a wavelength sensitivity (WS) of 15,000 nm/RIU and an amplitude sensitivity (AS) of 442.47 RIU-1 within a refractive index range of 1.22-1.33 [38]. Resonant wavelength (RW) variations can therefore be significantly influenced by an ITO layer.

We may obtain the Drude-Lorentz equation and associated parameters from the ITO ellipsometry data by using

$$\varepsilon_{ITO} = \varepsilon_b - \frac{{\omega_p}^2}{\omega(\omega + i\gamma_p)} + \frac{f_1{\omega_1}^2}{({\omega_1}^2 - \omega^2 - i\omega\gamma_1)} \quad (1)$$

In this context, $\varepsilon_{ITO}$ signifies the dielectric constant of ITO, $\omega_p$ denotes the plasma frequency, and $\varepsilon_b$ represents the polarization response of core electrons. Table 6.1 and 6.2 provides explicit numerical values for these parameters in Equation (1). The fact that Equation (1) holds true for wavelengths between 350 and 2000 nm should be emphasized. Consequently, it is best to ignore wavelengths outside of this range, which include the spectrum related to interactions between light and the ITO layer.

**Table 6.1:** Sellmeier Constants for Fused SIlica

| **Sellmeier Constants** | |
|---|---|
| $B_1$ | 0.696 |
| $B_2$ | 0.408 |
| $B_3$ | 0.897 |
| $C_1$ ($\mu m^2$) | 0.0047 |
| $C_2$ ($\mu m^2$) | 0.014 |
| $C_3$ ($\mu m^2$) | 97.934 |

**Table 6.2:** Drude-Lorentz Parameters for (10% wt) ITO

| | |
|---|---|
| $\varepsilon_b$ | 3.528 |
| $\omega_p[eV]$ | 1.78 |
| $\gamma_p[eV]$ | 0.155 |
| $f_1$ | 0.3884 |
| $\omega_1[eV]$ | 4.210 |
| $\gamma_1[eV]$ | 0.0919 |

Plasmonic materials that are widely used and prized for their diverse range of uses include gold and silver. Because of its lower cost and better-quality factor performance, silver is used in our work instead of gold because it exhibits a much stronger resonance peak than other plasmonic materials. Silver minimizes low optical damping and prevents interband transitions, just like gold does [39]. Silver, however, is easily oxidized and corroded, and when metal comes into contact with water, it forms fragile oxide layers [40], [41]. In order to address these problems and improve performance, we apply titanium dioxide (TiO2) to the silver layer [42]. Core-guided evanescent fields are more attracted to the outside due to the notable electron buildup caused by the special characteristics of TiO2 at the metal-insulator interface [43]. This large refractive index rise causes the sensor's sensitivity to shift toward the near-infrared (NIR) band in addition to encouraging improved mode interaction.

The dielectric constant of silver can be computed using the Drude-dispersion model and is provided as

$$\varepsilon_{Ag} = 1 - \frac{\lambda^2 \lambda_C}{\lambda_p{}^2 (\lambda_c + i\lambda)} \tag{2}$$

In this context, $\varepsilon_{Ag}$ stands for the wavelength in vacuum, $\lambda$ represents the dielectric constant of silver, and $\lambda_C$ indicates the collision wavelength of 17.614 μm. The plasma wavelength is 0.14541 μm.

The following equation is used to compute the relationship between RI and the wavelength of light:

$$n_{TiO_2} = \sqrt{5.913 + \frac{0.2441}{\lambda^2 - 0.0803}} \tag{3}$$

In this context of equation (3), $n_{TiO_2}$ stands for the RI of the $TiO_2$ layer, $\lambda$ represents light wavelength.

The analyte layer is positioned on the exterior of the fused silica covering to enable external sensing. A PML layer (perfectly matched layer), which absorbs all radiated energy, is included onto the analyte layer's outside to prevent radiation from escaping the computational zone.

The Sellmeier equation is used to calculate the RI profile of the fused silica utilized in the inner cladding:

$$n(\lambda) = \sqrt{1 + \frac{B_1\lambda}{\lambda^2 - C_1} - \frac{B_2\lambda^2}{\lambda^2 - C_2} - \frac{B_3\lambda^2}{\lambda^2 - C_3}} \tag{4}$$

In this context, $n(\lambda)$ stands for the RI of silica, $\lambda$ represents wavelength (μm). Table 6.1 holds rest of the values.

Our sensor's unique structural design and incorporation of plasmonic materials add uniqueness to our research. According to the literature currently in publication, no earlier research has investigated the use of ITO in conjunction with an Ag/TiO2 bimetallic layer in the same sensor arrangement.

**Table 6.3:** Initial Sensor Parameters

| **Parameter** | **Initial Value (nm)** |
|---|---|
| ITO Layer Width | 30 |
| Ag Layer Width | 30 |
| TiO2 Layer Width | 5 |
| Air Hole Width | 2000 |
| Pitch, p | 2000 |

Using COMSOL Multiphysics 5.6 software, the Finite Element Method (FEM) is used to do the numerical analysis.

## 6.4 Dispersion in the Sensor

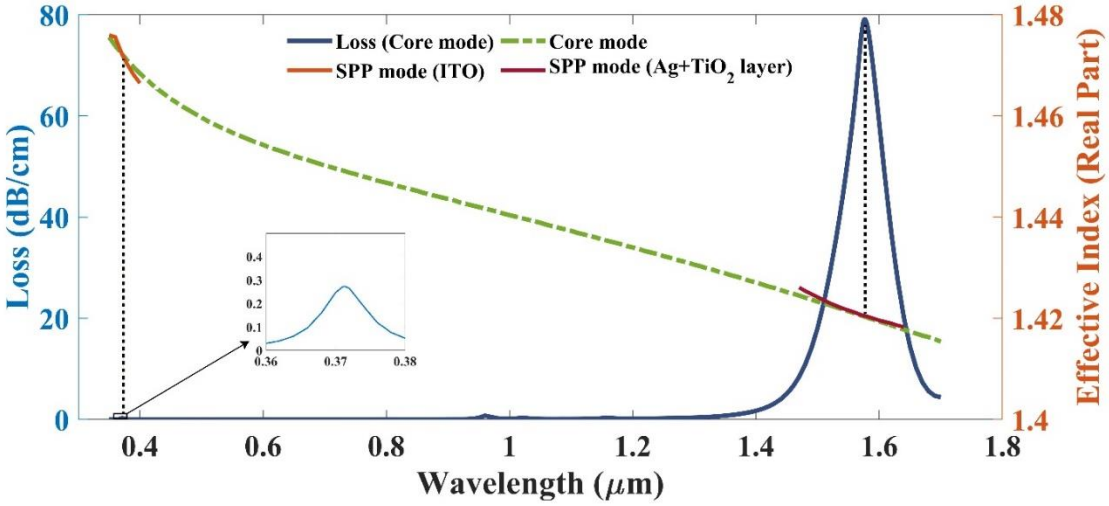


(a)

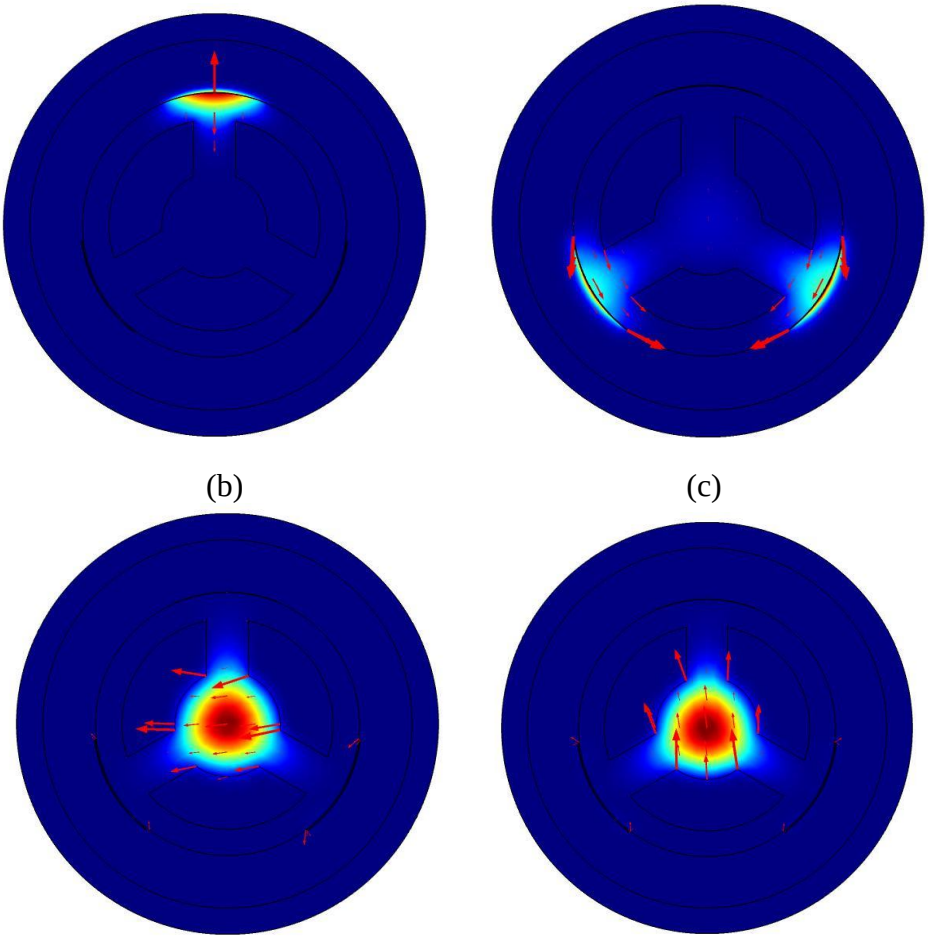

(b) (c)

(d) (e)

**Figure 6.2**: (b) Surface plasmon polariton (SPP) along the ITO layer, (c) SPP mode along the Ag+TiO2 layer, (d) x-polarization, (e) y-polarization for an analyte refractive index (RI) of 1.37

The frequency of the evanescent field and the alignment of electron frequencies in the sensor's plasmonic material must match. In order to maximize light confinement within the fiber, resonance must be achieved by synchronizing the effective indices of both modes at a certain wavelength. However, because of confinement, this resonance condition might result in a rise in peak loss.

The sensor consists of two separate Ag and TiO2 bimetallic layers as well as a thin layer of ITO. Two distinct Surface Plasmon Polariton (SPP) modes are produced by this combination, which causes an evanescent field to split into two halves. Because of the special qualities of silver and ITO, these modes interact over a large frequency range. As a result, when phase-matching requirements are met, two unique peaks emerge, preventing different resonance wavelengths for both polarization states. The SPP modes, as shown in Figure 6(b), 6(c), match the distinct plasmonic layers at particular wavelengths, confirming that the sensor's first peak is associated with the ITO layer and the second peak is a result of the bimetallic layer arrangement of titanium dioxide and silver.

## 6.5 Optimization of Sensor Parameters

Efficient optimization of the sensor's parameters is essential to maximizing its performance. We suggest using a dual strategy in this work called the Wavelength-Double Peak Shift (W-DPS) interrogation method. The sensor's Wavelength Sensitivity (WS) is assessed using this method in the following ways [48]:

$$S_{\lambda} = \Delta\lambda_{peak} / \Delta n_a \, (nm / RIU) \tag{5}$$

In this context, $S_{\lambda}$ stands for wavelength sensitivity, $\Delta\lambda_{peak}$ represents the displacement of the two resonant wavelengths consecutively, and $\Delta n_a$ indicates the variation in RI.

The following formula is used to measure the confinement loss (CL) spectra [48]

$$\alpha(dB / cm) = 8.686 \times (\frac{2\pi}{\lambda}) \times \mathrm{Im}(n_{eff}) \times 10^4 \tag{6}$$

On the other hand, the following formula is used to determine Double Peak Shift Sensitivity (DPSS), a specific version of the WS parameter that is applied to sensors made with two different plasmonic materials [32]:

$$S_{p-p} = \frac{(\lambda_{p2} - \lambda_{p1})_{n_b} - (\lambda_{p2} - \lambda_{p1})_{n_a}}{n_b - n_a} \times 10^3 (nm / RIU) \quad (7)$$

In this context, $S_{p-p}$ denotes the Double Peak Shift Sensitivity at RI 1.36, and $\lambda_{p1,n_a}$, $\lambda_{p1,n_a}$ represents the wavelength of the 1st peak at RI 1.36, and $\lambda_{p2,n_b}$, $\lambda_{p2,n_a}$ depict the wavelengths of the 2nd peaks at RIs 1.36 and 1.37, respectively.

Sensor parameters are selected to maximize both the Wavelength Sensitivity (WS) and Double Peak Shift Sensitivity (DPSS).

Using the y-polarization mode, optimization was carried out for refractive indices (RI) of 1.36 and 1.37. Using the starting values described in Section II, 2397 nm/RIU was found to be the Double Peak Shift Sensitivity (DPSS). It was discovered that the two peaks' associated Wavelength Sensitivity (WS) values were 1172 nm/RIU and 3569 nm/RIU, respectively.

### *6.5.1 Width of ITO Layer*

The optimization first concentrated on the ITO layer. Raising the distance between the two peaks was crucial to optimizing the system's Double Peak Shift Sensitivity (DPSS). The first peak is shifted towards higher wavelengths when the ITO layer thickness increases, lowering the DPSS. As a result, the ITO layer's thickness was gradually decreased starting at 30 nm and increasing every 5 nm. The resonance wavelength (RW) associated with the ITO layer at a thickness of 15 nm was found to be 367.275 µm at RI=1.36. A larger reduction would have caused the RW to change before the 350 nm cutoff. Since the range of Equation 1 is limited to 350 nm to 2000 nm, 15 nm was chosen as the ideal thickness.

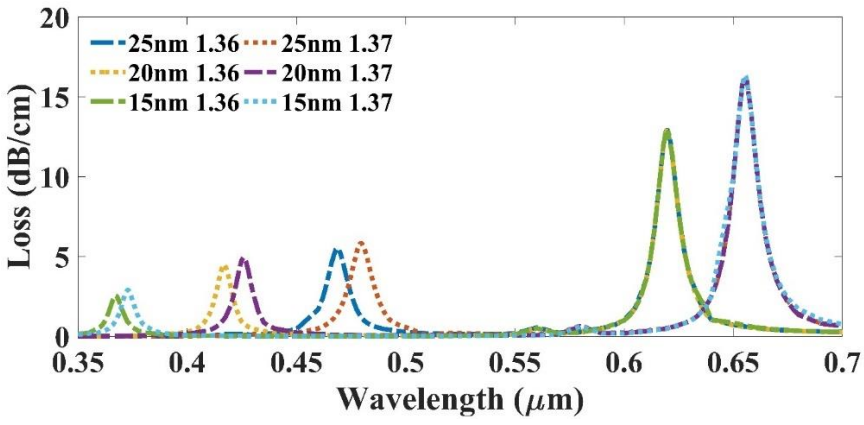

(a)

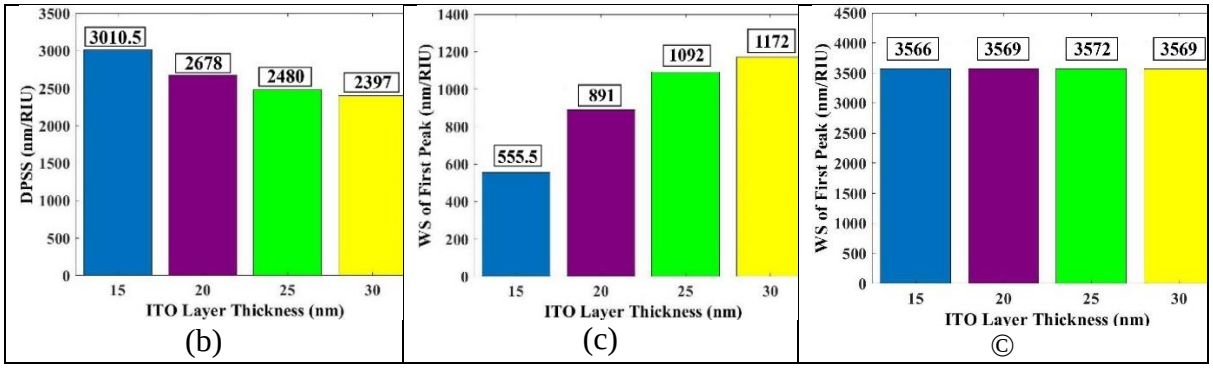


**Figure 6.3:** (a) The plot of CL versus wavelength for different $t_{ITO}$ at Refractive Indices 1.36 & 1.37, (b) The impact of DPSS with different $t_{ITO}$, (c) WS of the first peak, and (d) WS of the second peak

It is clear from Figure 6.3(b) that the DPSS rises as the ITO layer's width falls. With this modification, the Wavelength Sensitivity (WS) of the second peak varies very little. Furthermore, Figure 6.3(a) shows that when thickness decreases, the coupling length (CL) of the first peak decreases.

Following ITO layer optimization, the DPSS value increased to 3010.5 nm/RIU. The detection range was increased by this modification from 367.275 nm to 619.755 nm wavelength.

### *6.5.2 Width of Ag Layer*

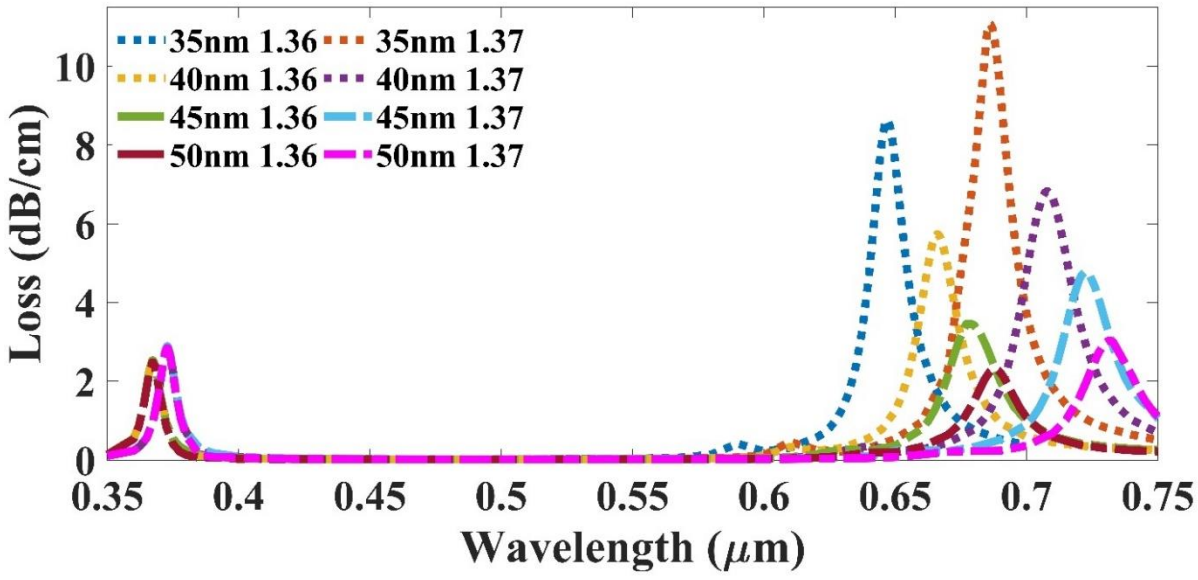


(a)

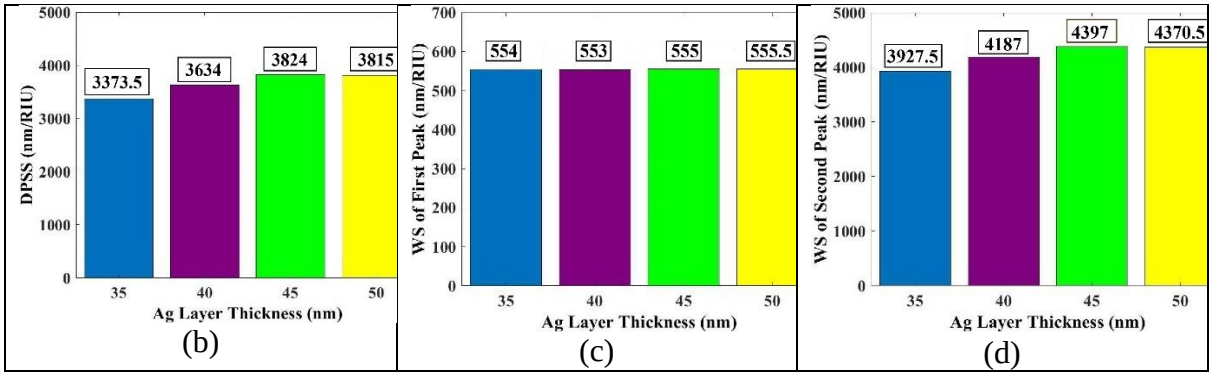


**Figure 6.4:** (a) The plot of Coupling Length (CL) versus wavelength for varying $t_{Ag}$ at Refractive Indices 1.36 & 1.37, (b) The impact of Double Peak Shift Sensitivity (DPSS) with different $t_{Ag}$ , (c) Wavelength Sensitivity (WS) of first peak, and (d) WS of second peak

The Ag layer was the focus of the optimization after that. The resonance wavelength (RW) shifts to the right as the Ag film's width increases. In order to maximize the Double Peak Shift Sensitivity (DPSS), we set out to determine the thickness at which the Wavelength Sensitivity (WS) of the second peak reaches its maximum.

We gradually expanded the Ag layer width to 50 nm from a starting point of 30 nm. With a corresponding DPSS of 3824 nm/RIU, the second peak's WS rose progressively to a width of 45 nm, achieving a value of 4379 nm/RIU. The DPSS attained was 3815 nm/RIU, however at 50 nm, the WS dropped to 4370.5 nm/RIU. As we can see from figure 6.4(c), the first peak barely affects the value variation. The rise in led to an increase in the detection range to 678.71 nm.

### *6.5.3 Width of $TiO_2$ film Layer*

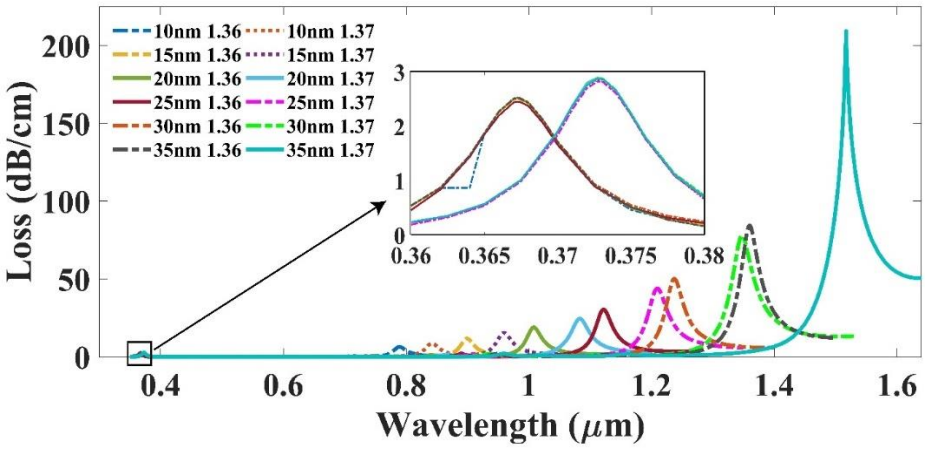


(a)

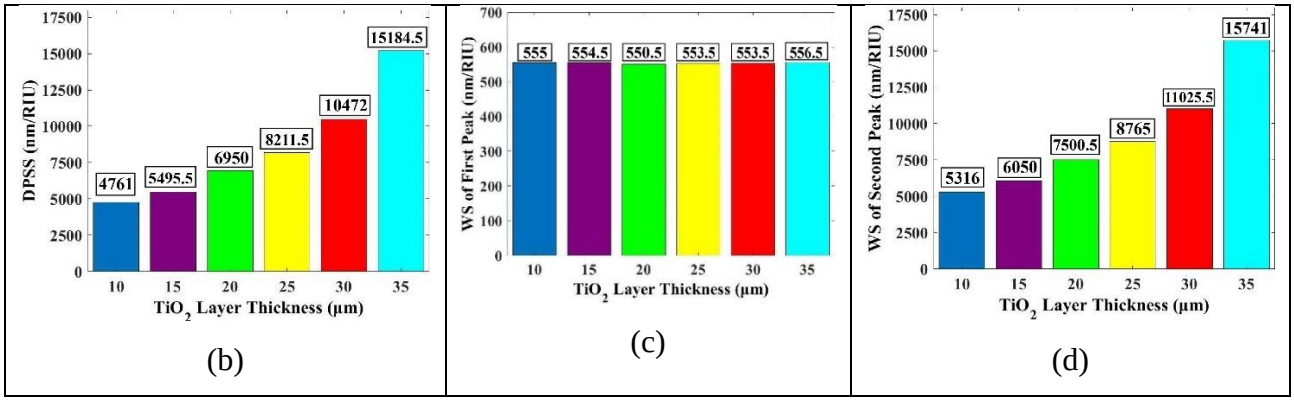


**Figure 6.5**: (a) The plot of Coupling Length (CL) versus wavelength for varying $t_{TiO_2}$ at Refractive Indices 1.36 and 1.37, (b) The impact of Double Peak Shift Sensitivity (DPSS) with different $t_{TiO_2}$, (c)Wavelength Sensitivity (WS) of the first peak, and (d) WS of the second peak

The TiO2 film was first applied mainly to prevent oxidation of the silver layer. But when looking at the bimetallic layer as a whole, it was found that the TiO2 film also greatly improves the system's sensitivity [42]. In steps of five nm, the thickness of TiO2 was raised from its starting value. It was shown that the second peak's Double Peak Shift Sensitivity (DPSS) and Wavelength Sensitivity (WS) both significantly improved as they grew.

The combined bimetallic layer of silver and TiO2 attained a total thickness of 80 nm at 35 nm. As a result, it was difficult to effectively couple the core mode and the Surface Plasmon Polariton (SPP). The phase matching criterion became more difficult to achieve as the amount increased, eventually to the point where the resonance condition could no longer be maintained. Thus, 35 nm was found to be the ideal thickness for the TiO2 coating.

The spectrum reaches into the optical communication band in Figure 6.4(a). Resonance wavelength (RW) is at 1395.77 nm at RI of 1.36 and shifts to 1517.18 nm at RI of 1.37. This shows that within the optical communication range, the sensor covers both the E-band and S-band.

### *6.5.4 Air Hole Width and Pitch*

Modifying the air hole width involved making 100 nm increments and decreases. The Double Peak Shift Sensitivity (DPSS) decreased to 10865.5 nm/RIU with a 100 nm width increase, while the Wavelength Sensitivity (WS) values for the first and second peaks were 508.5

nm/RIU and 11374 nm/RIU, respectively. However, reducing the breadth resulted in an enormous gap between the plasmonic layers and the air holes, which made it challenging to meet the phase matching criterion required for resonance. As a result, the preset value of 2 µm was found to be the ideal width for the air holes.

Next, in order to maximize the second peak's WS and DPSS, the pitch—the separation between two neighboring air holes—was modified. Pitch increase increased the Coupling Length (CL) and, as a result, the DPSS and WS dropped together with a smaller spacing between the resonance wavelengths (RWs). In contrast, the air holes grew closer together as the pitch decreased, lowering the CL. DPSS and WS both rose when the pitch lowered, as seen in figures 6.6 (b), (c), and (d).

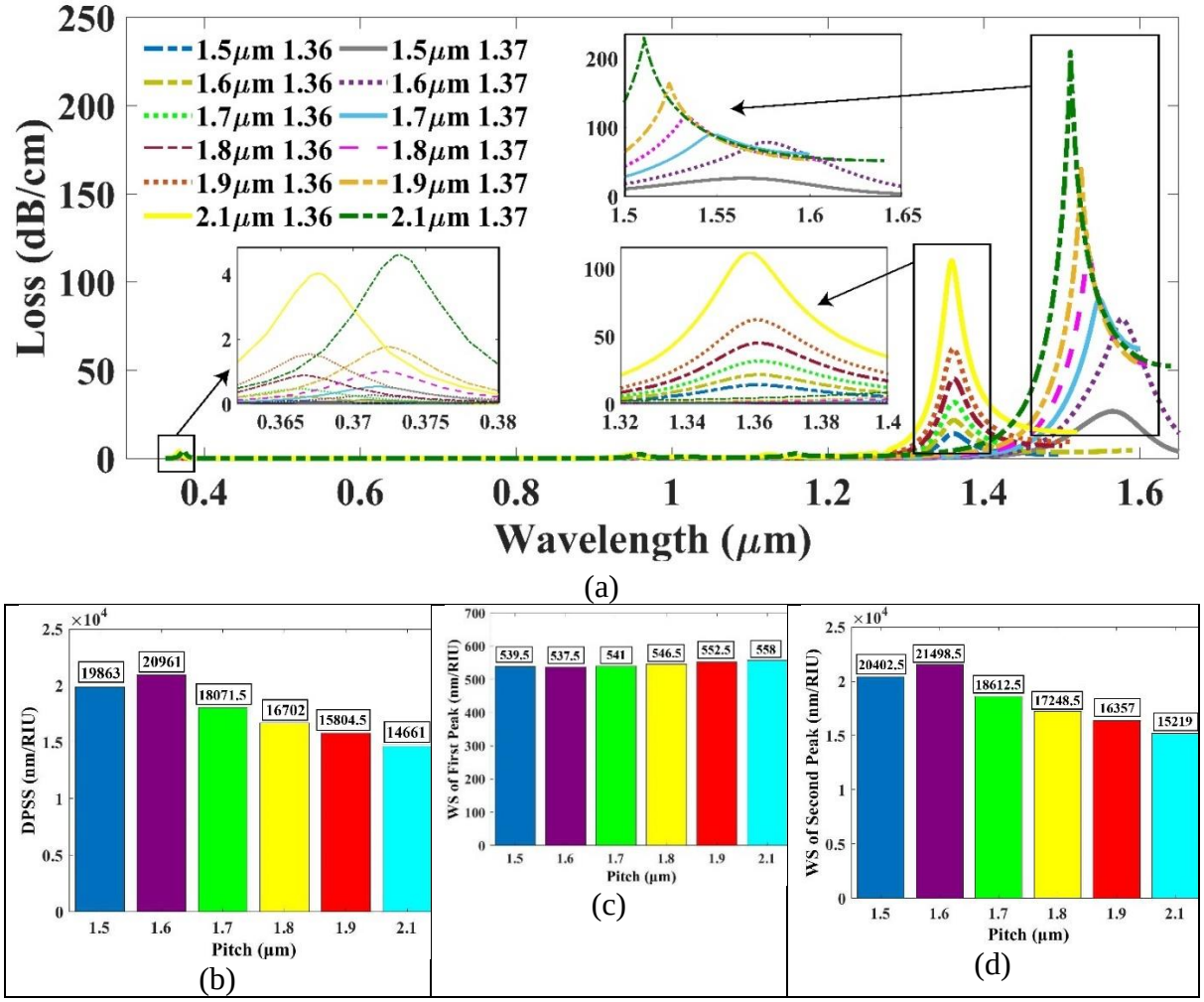


**Figure 6.6:** (a) Plot of CL vs wavelength for different pitch values at Refractive Indices of 1.36 and 1.37 (b) Impact of different pitch on DPSS (c) WS of the first peak and (d) WS of the second peak

Resonant wavelengths for RIs of 1.36 and 1.37 were found at 1361.495 nm and 1576.48 nm, respectively, at the maximum shift, which was detected at a pitch value of 1.6 µm. The application of the sensor is expanded into the optical spectrum's L-Band with this modification.

**Table 6.4:** Optimized Sensor Performance Parameters

| **Name of Parameter** | **Width Initially (nm)** | **Width Finally (nm)** | **DPSS (after Optimization, in nm/RIU)** | **WS (after Optimization, in nm/RIU)** |
|---|---|---|---|---|
| $t_{ITO}$ | 30 | 15 | 3010.5 | 3566 |
| $t_{Ag}$ | 30 | 45 | 3824 | 4379 |
| $t_{TiO_2}$ | 5 | 35 | 15184.5 | 15741 |
| $w_{air}$ | 2000 | 2000 | 15184.5 | 15741 |
| $p$ | 2000 | 1600 | 20961 | 21498.5 |

# Chapter 7

# Analysis of the Presented Sensor's Performance Parameters

## 7.1 Introduction

This chapter examines the performance metrics of the open core PCF sensor that resembles a wheel. To comprehend the sensor's effectiveness and suitability for a range of sensing applications, this examination is essential.

The important performance parameters taken into account in this study are:

- Double Peak Sensitivity Shift (DPSS)
- Wavelength Sensitivity (WS)
- Amplitude Sensitivity (AS)
- Sensor resolution
- Linearity
- Figure of Merit (FOM)

Every metric is thoroughly analyzed to offer a thorough assessment of the sensor's strengths and weaknesses. The goal of this chapter is to provide a comprehensive knowledge of how these performance characteristics affect the suggested sensor design's overall usefulness and efficacy.

## 7.2 DPSS

Double Peak Sensitivity Shift (DPSS) gauges how different refractive indices affect the sensitivity between two resonance peaks.

For both x- and y-polarization, the sensor we designed shows distinct dual peaks within RI ranges of 1.35-1.38 and 1.32-1.38, respectively. Equation (7) of Section 6.5 in Chapter 6 was utilized by the sensor to attain a remarkable DPSS of 50,000 nm/RIU at a RI of 1.37 along the y-polarization. 45,503 nm/RIU was the maximum DPSS for x-polarization that was measured. These numbers establish a new standard, considerably exceeding the greatest DPSS ever

recorded, which was 27,341.5 nm/RIU. It is significant to note that because the resonance state of the ITO layer exceeded the 350 nm limit given by equation (1), the sensor was not tested for x-polarization before a RI of 1.35 or for y-polarization before a RI of 1.32 [37].

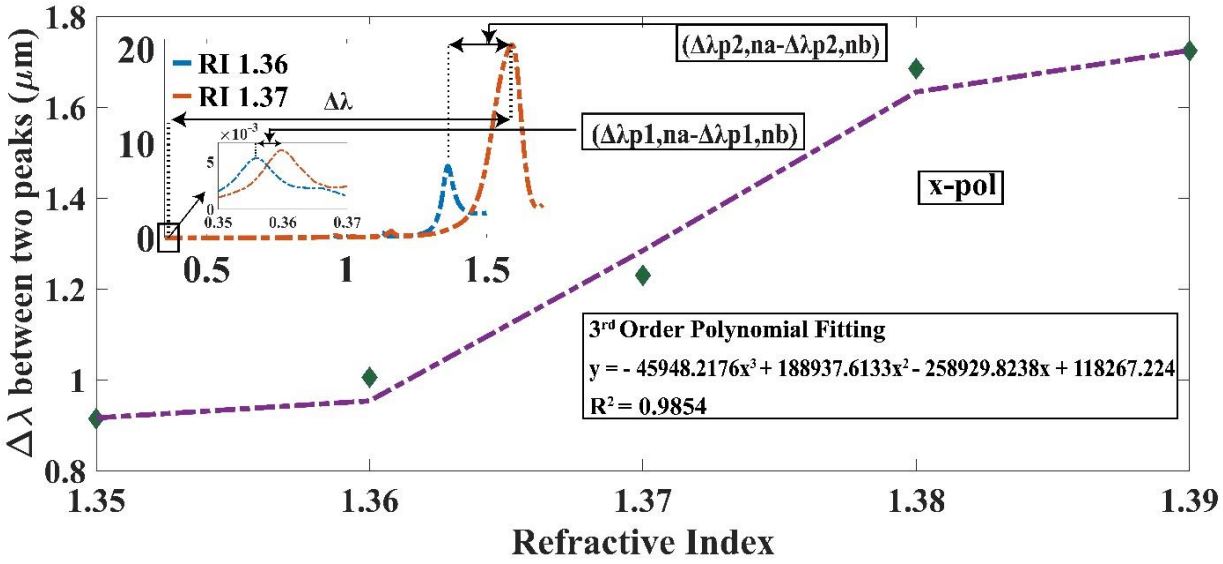


(a)

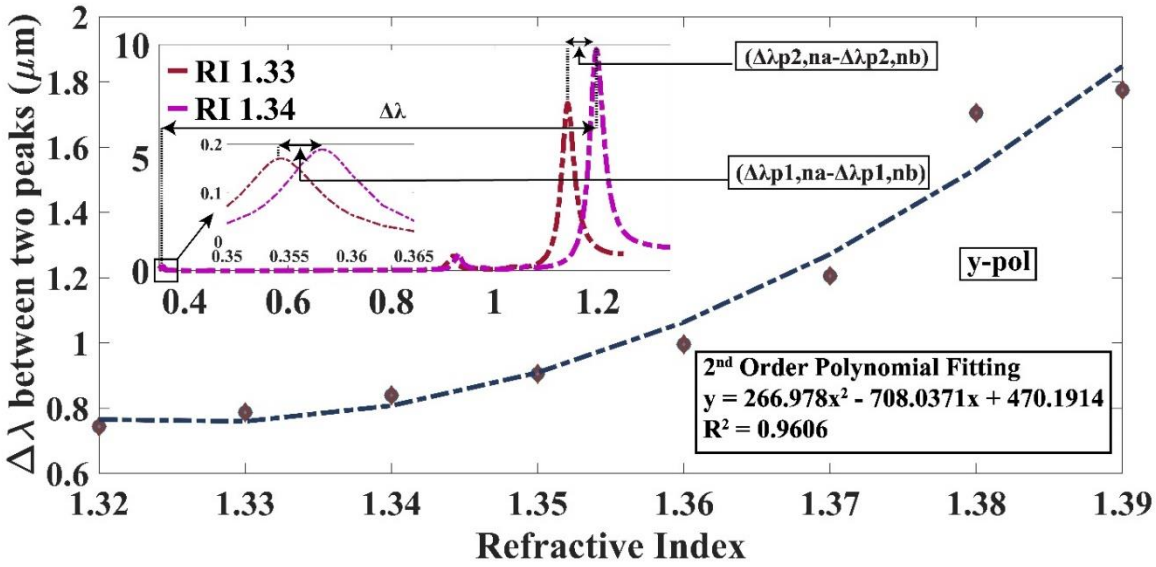


(b)

**Figure 7.1:** Variation in RW along both of the polarizations

Due to variations in the loss strength between the resonance peaks, which are mostly brought on by light scattering events, the energy transfer between the two modes changes with wavelength. As can be seen in Figure 9, there are less losses in the x-polarization mode than in the y-polarization mode. In particular, at a RI of 1.38, the x-polarization mode exhibits the largest loss difference between the two peaks at 94.2346 dB/cm, whereas the y-polarization

mode displays a loss difference of 158.4287 dB/cm at the same RI. Figures 8 and 10 show that the RW shifts down to a RI of 1.38, which is the point at which the investigation for both polarizations ends. The sensor's range for x-polarization is 350 nm to 2094.79 nm, and for y-polarization, it is 2160.88 nm.

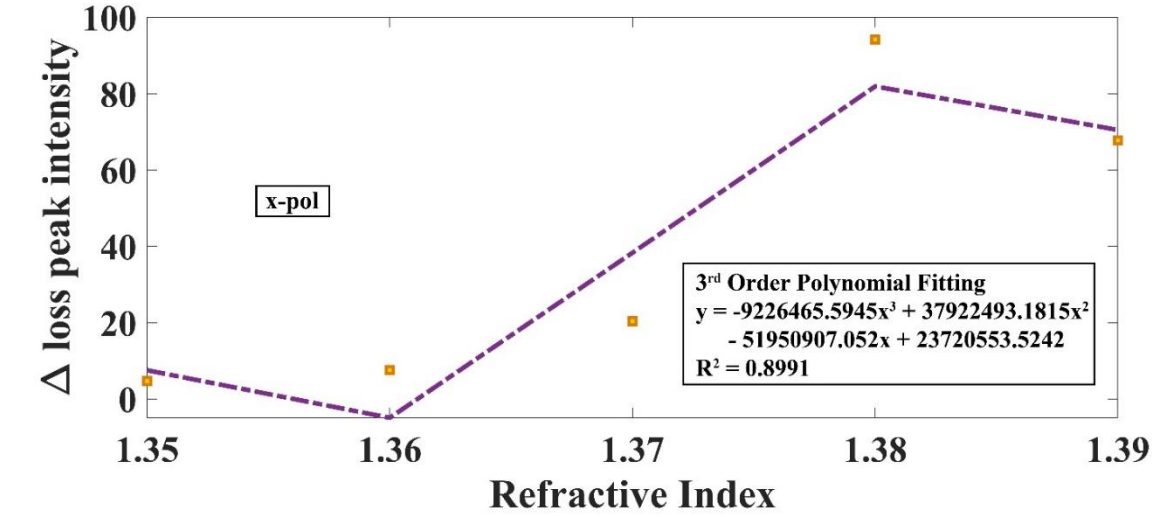


(a)

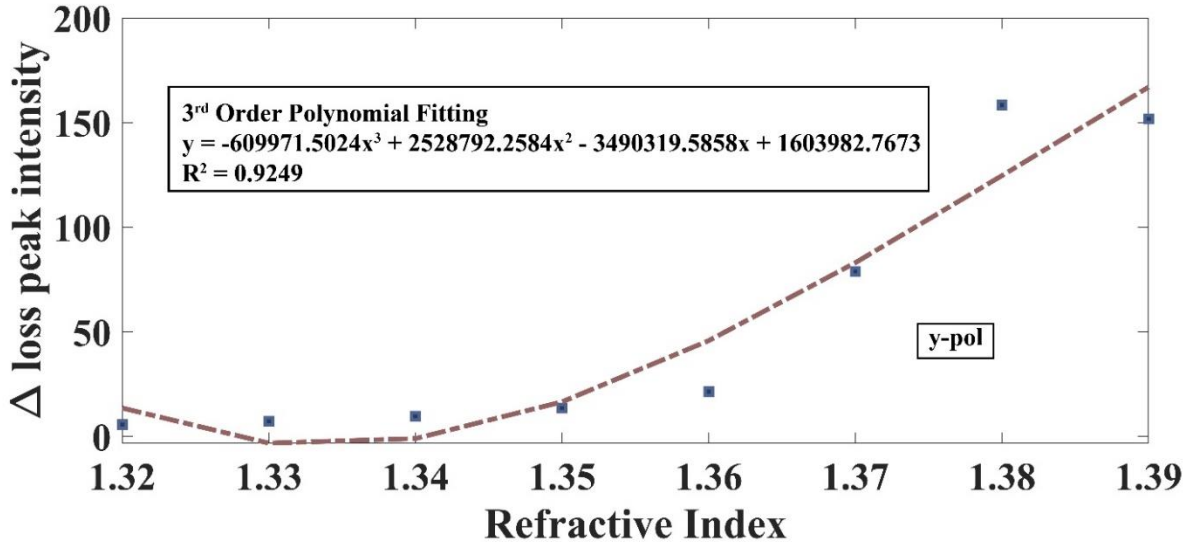


(b)

**Figure 7.2:** Association between Refractive Index and the variation in the peak strength of loss in both polarizations

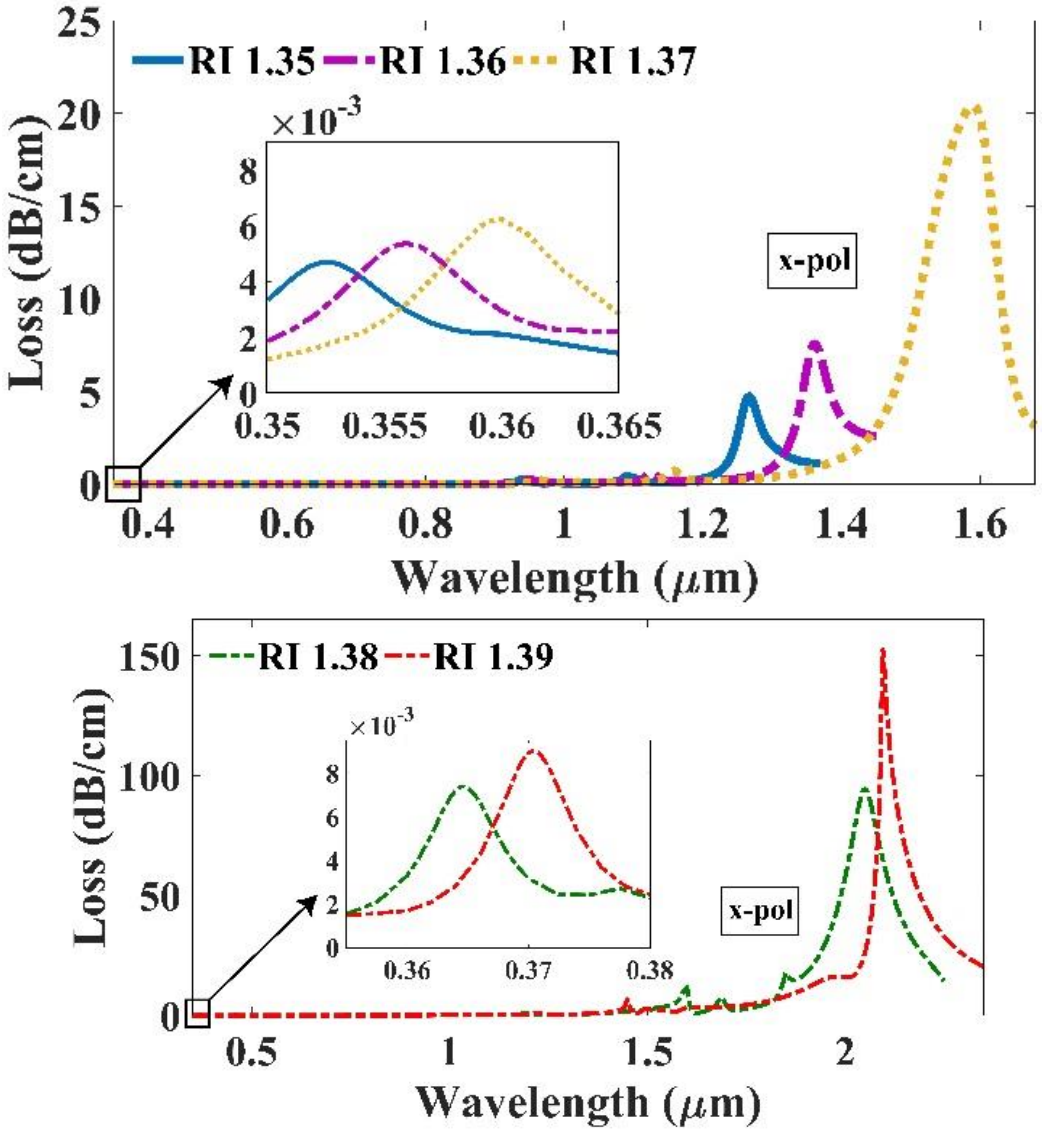
RI 1.35
RI 1.36
RI 1.37
×10^-3
x-pol
Loss (dB/cm)
Wavelength (μm)
RI 1.38
RI 1.39
×10^-3
x-pol
Loss (dB/cm)
Wavelength (μm)

(a)

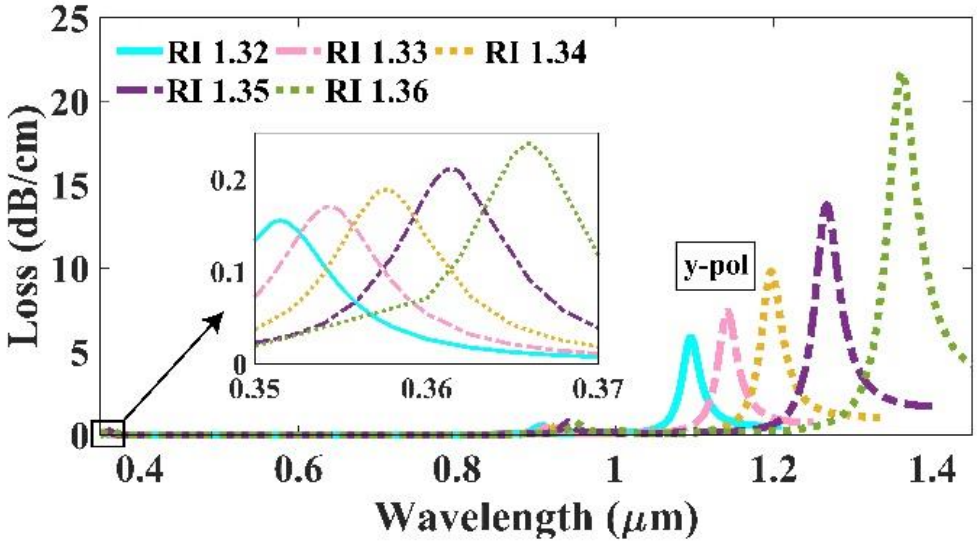
RI 1.32
RI 1.33
RI 1.34
RI 1.35
RI 1.36
y-pol
Loss (dB/cm)
Wavelength (μm)

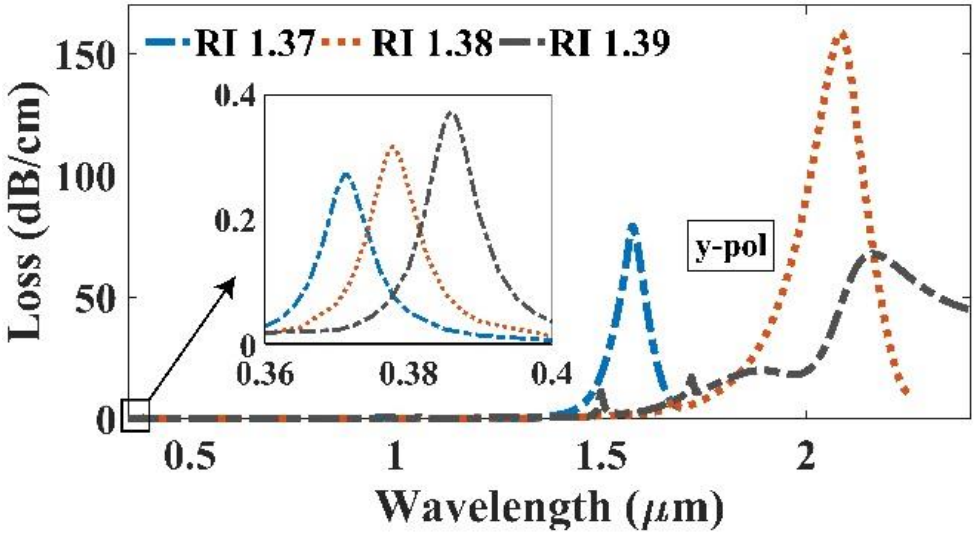


(b)

**Figure 7.3:** The coupling length (CL) plotted against wavelength for (a) x-polarization within the range of 1.35-1.39 RI, and (b) y-polarization from 1.32-1.39 RI

## 7.3 WS

The sensor's capacity to modify its resonant wavelength in response to variations in the refractive index is indicated by its wavelength sensitivity (WS).

The sensor's WS was examined for both polarizations using equation (5) of Section 6.5 in Chapter 6. Since the first peak's function was to improve the distinction between the two peaks at the same refractive index, we specifically concentrate on the WS of the second peak. For both x- and y-polarization, our sensor reaches maximum WS values of 45,978.5 nm/RIU and 50,652 nm/RIU at RI = 1.37. This demonstrates how the significant shift in resonant wavelength allows the sensor to detect analytes with accuracy. But the WS drastically drops to 4500 nm/RIU for x-polarization and 7788 nm/RIU for y-polarization at RI 1.38. As a result, the inquiry was stopped at this refractive index.

## 7.4 AS

A sensitivity metric that takes into consideration light attenuation at a specific wavelength is called amplitude sensitivity, or AS. This equation is used to calculate it [31]:

$$S_A = -\frac{1}{\alpha(\lambda, n_a)} \frac{\partial_a(\lambda, n_a)}{\partial n_a} (RIU^{-1}) \tag{8}$$

This method saves money because it does not require light interaction. For x-pol at RI 1.37 and y-pol at RI 1.36, our suggested sensor exhibits peak AS values of 1166.7435 $RIU^{-1}$ and 1668.34 $RIU^{-1}$, respectively. We have to stop measuring the AS after these refractive indices because it starts to decrease after that.

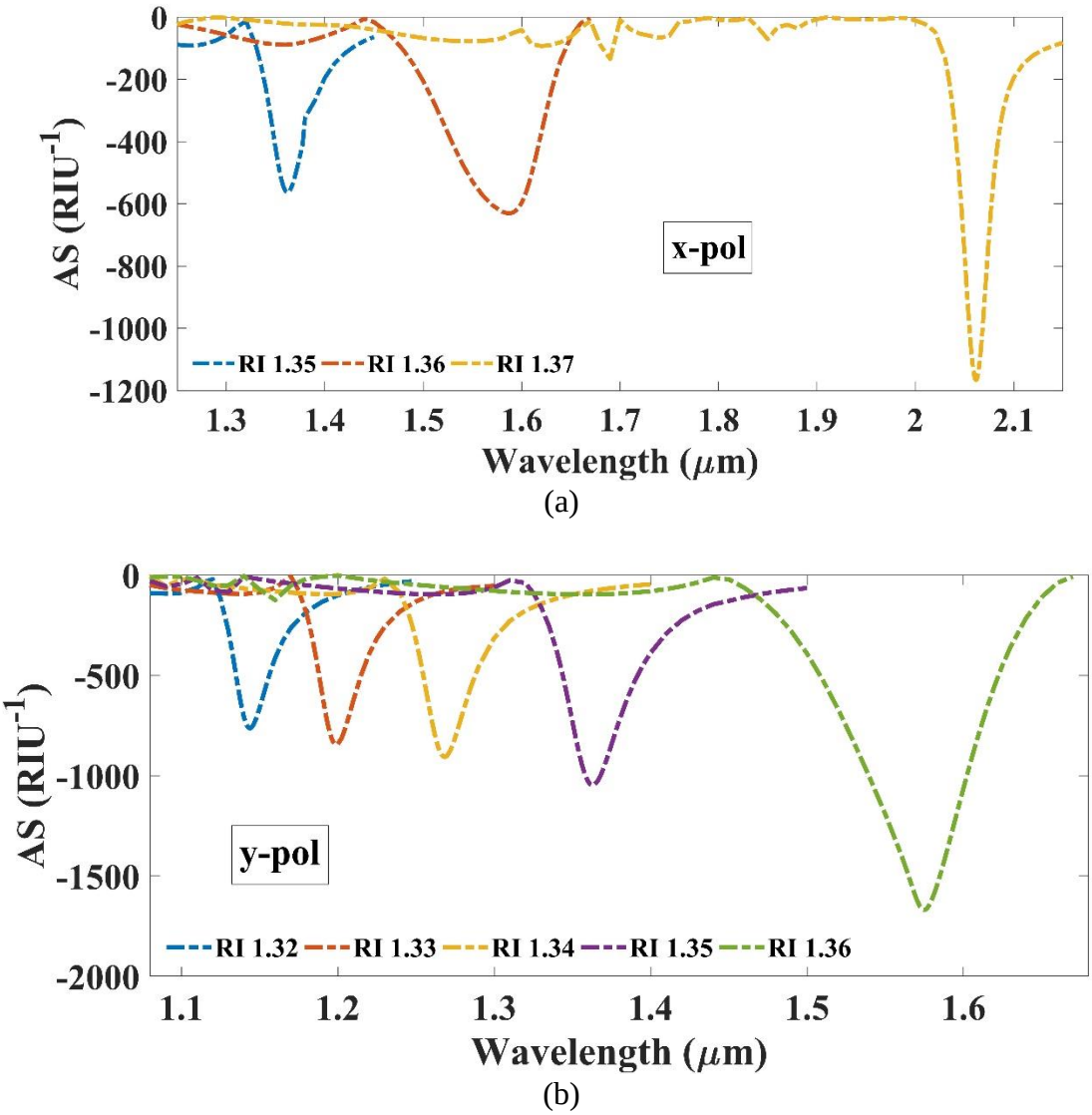


**Figure 7.4:** AS in both x and y polarization

## 7.5 Sensor's Resolution

A crucial requirement for reliably identifying analytes is sensor resolution, especially when identifying subtle variations in the analyte's refractive index (RI). This is the smallest change

in refractive index that can be detected and measured with accuracy by the sensor.Equations (9) and (10) provide instructions on how to calculate it using the measuring techniques of wavelength sensitivity (WS) and amplitude sensitivity (AS) [32]:

$$R_A = \frac{\Delta n_A}{S_A}(RIU) \tag{9}$$

$$R(w) = \frac{\Delta \lambda_{\min}}{S_\lambda}(RIU) \tag{10}$$

In this context, $R_A$ stands for Amplitude Resolution (RIU), $S_A$ represents amplitude sensitivity ($RIU^{-1}$), $R(w)$ is Wavelength Resolution (RIU), and lastly $S_\lambda$ here is WS (nm/RIU).

The resolution of amplitude was $8.571\times10^{-6}$ RIU along the x-polarization and $5.994\times10^{-6}$ RIU along the y-polarization. In terms of wavelength resolution, $2.175\times10^{-6}$ RIU was obtained by the x-polarization, whereas $1.974\times10^{-6}$ RIU was obtained by the y-polarization. As a result, our sensor shows that it can pick up on minute changes on the $10^{-6}$ scale.

## 7.6 Linearity

The term "linearity" refers to the sensor's response constancy across a variety of refractive indices.

A high correlation between the resonance wavelength (RW) and the refractive index (RI) of the material under study suggests the possibility of a highly precise and readily calibrable sensor. The RW vs RI plot for x-polarization has an $R^2$ of 0.9333 and is linearly related to the equation y = 23.44x – 30.44. The $R^2$ value increases to 0.9854 when a third-order polynomial equation is applied to the scatter plot. The linear fit produces the equation y = 15.95x – 20.13 with an $R^2$ of 0.863 in the case of y-polarization. On the other hand, the $R^2$ value rises to 0.9817 when the polynomial order is raised to the fourth degree. The excellent quality of our sensor is demonstrated by this analysis, as shown in Figures 7.5 (a) and (b).

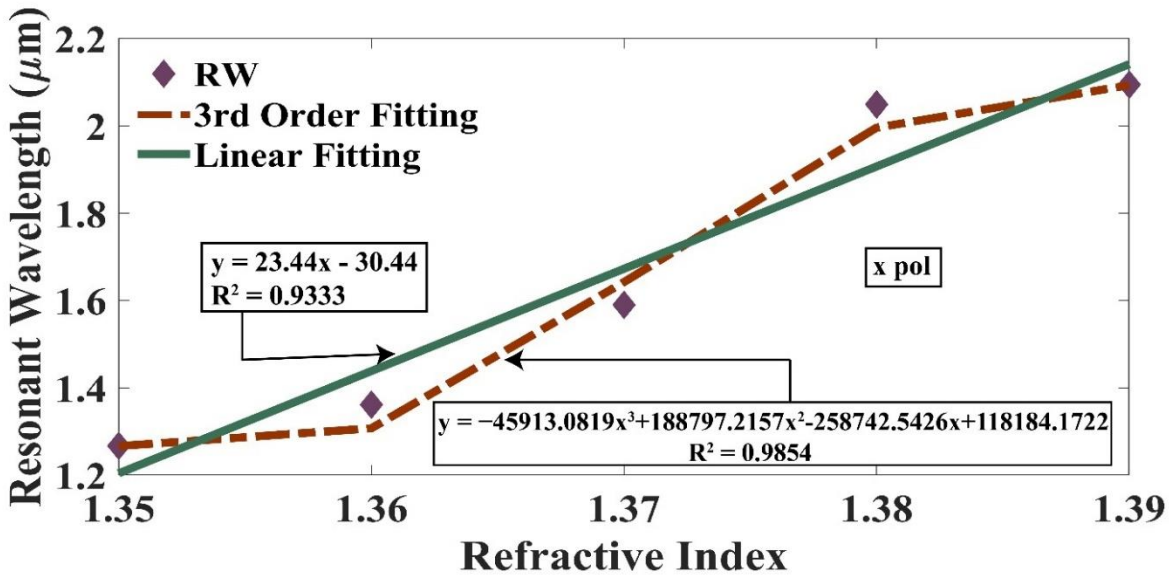


(a)

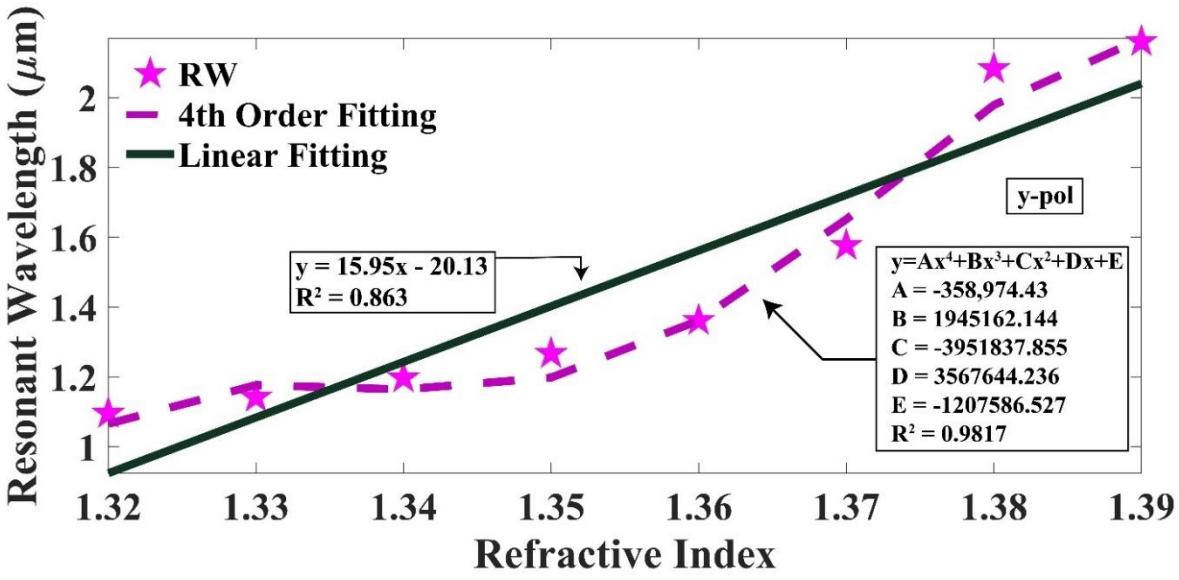


(b)

**Figure 7.5:** Modeling the Ag peak using polynomials in both x and y polarizations

## 7.7 FOM (Figure of Merit)

Figure of Merit (FOM) is a thorough metric that assesses the sensor's overall performance by combining sensitivity and resolution. This parameter (FOM) is calculated using the equation below [48]:

$$FOM = \frac{S_\lambda}{FWHM}(RIU^{-1}) \tag{11}$$

Here Full Width at Half Maximum is indicated by FWHM. Our sensor shows a high Figure of Merit (FOM) of 1017.108 $RIU^{-1}$ along the y-polarization and 421.05 $RIU^{-1}$ along the x-polarization. Among silver-based sensors, the notably high FOM along the y-polarization is a unique property that is never observed.

| RI | RW (nm) | WS (nm/RIU) | AS ($RIU^{-1}$) | DPSS (nm/RIU) | Wavelength Resolution (RIU) ($\times 10^{-6}$) | Amplitude Resolution (RIU) ($\times 10^{-6}$) | FOM ($RIU^{-1}$) |
|---|---|---|---|---|---|---|---|
| 1.35 | 1266.98 | 9451.5 | 563.18 | 9115 | 10.58 | 17.756 | 203.7 |
| 1.36 | 1361.49 | 22851.5 | 630.47 | 22454.5 | 4.376 | 15.86 | 382.07 |
| 1.37 | 1590.01 | 45978.5 | 1166.74 | 45503 | 2.175 | 8.57 | 421.05 |
| 1.38 | 2049.79 | 4499.5 | - | 3921.5 | 22.25 | - | 31.687 |

**Figure 7.6:** Performance characteristics of the sensor at all examined refractive indices (x polarization)

| RI | RW (nm) | WS (nm/RIU) | AS ($RIU^{-1}$) | DPSS (nm/RIU) | Wavelength Resolution (RIU) ($\times 10^{-6}$) | Amplitude Resolution (RIU) ($\times 10^{-6}$) | FOM ($RIU^{-1}$) |
|---|---|---|---|---|---|---|---|
| 1.32 | 1095.16 | 4621.5 | 762.478 | 4336 | 21.64 | 13.115 | 163.94 |
| 1.33 | 7399.99 | 5548.5 | 844.177 | 5218.5 | 18.02 | 11.846 | 180.733 |
| 1.34 | 1196.86 | 6985 | 905.161 | 6602 | 14.32 | 11.048 | 204.24 |
| 1.35 | 1266.71 | 9478.5 | 1046.81 | 9031.5 | 10.55 | 9.553 | 236.667 |
| 1.36 | 1361.49 | 21499 | 1668.34 | 20961 | 4.65 | 5.994 | 431.697 |
| 1.37 | 1576.48 | 50652 | - | 50000 | 1.97 | - | 1017.11 |
| 1.38 | 2083 | 7788 | - | 6976 | 12.84 | - | 46.083 |

**Figure 7.7:** Performance characteristics of the sensor at all examined refractive indices (Y-POL)

# Chapter 8

# Applications and Novelty of the Projected Sensor

## 8.1 Introduction

The sensor that this study produced has great potential and versatility in a variety of applications. The sensor is ideal for a wide range of cutting-edge technical applications since it can operate in both the optical communication band and the mid-infrared (M-IR) region. Sensor applications include fiber-optic communications, telecommunications, sensing systems, and optical amplifiers. The sensor operates in the optical communication band, which is between 1260 and 1650 nm. High-speed, effective data transport with little signal degradation is ensured by the minimal attenuation within this spectral band.

Furthermore, the sensor's use in the M-IR range, which spans wavelengths from 1095 nm to 2160 nm, presents prospects for gas sensing, medical imaging, remote sensing, spectroscopy, and environmental monitoring. The sensor is especially useful in these domains because it can attain phase matching conditions over a wide wavelength range.

The sensor has great promise as a biosensor, even beyond these technological uses. It has special abilities for detecting biomolecules and biochemicals because of its ability to create resonance conditions over a wide range, from 350 nm to 2083 nm along the x-polarization and up to 2160 nm along the y-polarization. Significant potential for improvements in biochemical analysis, medical diagnostics, and other biosensing fields exists because to this wide detection range.

## 8.2 Utilization of the Sensor in M-IR Region and Optical Communication Bands

The term "optical communication band" describes a specific region of the electromagnetic spectrum that is mainly utilized for data transmission via light signals. This spectral band, which runs from 1260 to 1650 nm, was selected because optical fibers in this range show the

least attenuation from light scattering and absorption. As a result, there is little signal deterioration during high-speed, effective data transfer in this wavelength domain [49].

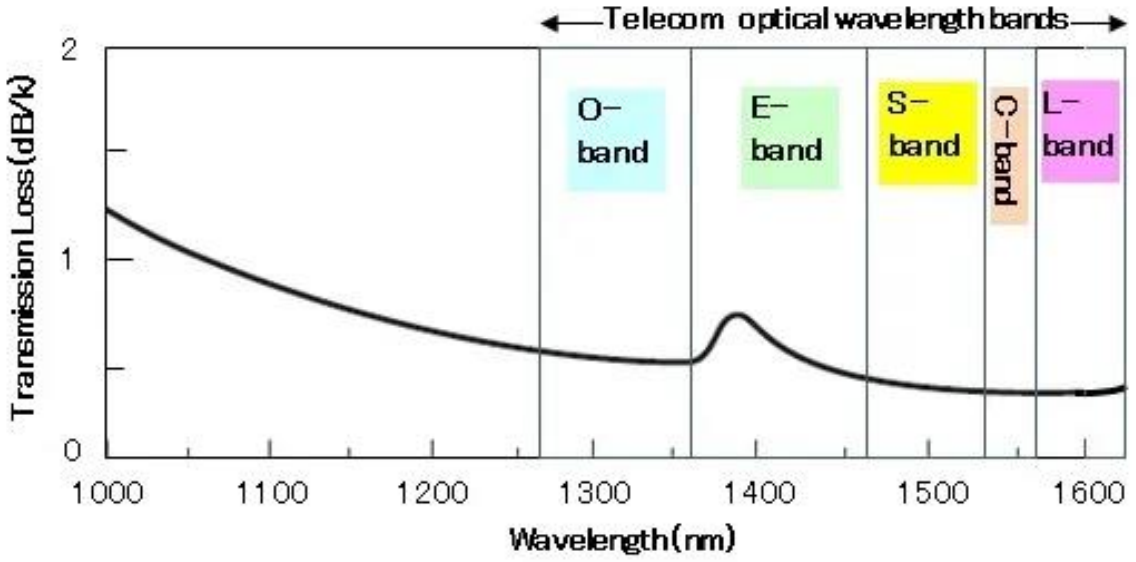


**Figure 8.1:** Optical Communication Bands broken into categories: O-band, E-band, S-band, C-band, and lastly, U-band

It is clear from Figure 7.6 and 7.7 that the resonant wavelength of our sensor's second peak ranges from 1095 nm to 2160 nm, encompassing the optical communication band as well as the mid-infrared (M-IR) band range. The sensor can be used in many different industries, including fiber-optic communications, optical amplifiers, sensing systems, and telecommunications, thanks to its wide coverage [50]. The sensor can also be used for spectroscopy, gas sensing, imaging in health care, remote sensing, and monitoring of the environment in the M-IR range [51], [52].

## 8.3 Potential of the Sensor in Bio-sensing

Due to its ability to create resonance conditions over a wide range, our sensor shows great promise as a biosensor. The sensor can specifically reach phase matching conditions up to 2160 nm along the y-polarization and 350 nm to 2083 nm along the x-polarization. These wider wavelength ranges have special qualities that make them appropriate for biomolecule and biochemical detection. Table 8.1 lists some applications for this skill.

**Table 8.1:** A Listing of Some Biochemicals And Biomolecules That are Within Our Sensor's Perimeter

| **Name of Prospective Analytes** | **RI of the Analyte** | **DPSS, in nm/RIU** | **WS, in nm/RIU** | **AS, in $RIU^{-1}$** |
|---|---|---|---|---|
| Methyl, Water | 1.33 | 5218.5 (y-pol) | 5548.5 (y-pol) | 844.17 (y-pol) |
| Milk, Plasma | 1.35 | 9115 (x-pol) | 9478.5 (y-pol) | 1046.81 (y-pol) |
| WBC, Basal cells, Acetone | 1.36 | 22454.5 (x-pol) | 22851.5 (x-pol) | 1668.34 (y-pol) |
| Acetic Acid | 1.37 | 50000 (y-pol) | 50652 (y-pol) | 1166.74 (x-pol) |
| Skin Cell | 1.38 | 6976 (y-pol) | 7788 (x-pol) | - |

## 8.4 Comparison of Our Sensor with Relevant Past Work Done

**Table 8.2:** Comparative evaluation within the framework of pertinent research

| **Ref.** | **Materials** | **RI range** | **AS, in $RIU^{-1}$** | **WS, in nm/RIU** | **WR, in RIU** | **AR, in RIU** | **FOM, in $RIU^{-1}$** | **DPSS, in nm/RIU** |
|---|---|---|---|---|---|---|---|---|
| [38] | ITO | 1.22 – 1.33 | 442.47 | 15,000 | - | $6.67*10^{-6}$ | - | - |
| [53] | ITO+ZnO | 1.30 – 1.38 | - | 10,000 | $2.0\times10^{-5}$ | - | - | - |
| [54] | Ag / Graphene | 1.46 – 1.49 | 418 | 3,000 | $3.33\times10^{-5}$ | $2.4*10^{-5}$ | - | - |
| [55] | Ag / Graphene | 1.33 – 1.35 | 72.47 | 2,520 | $3.97\times10^{-5}$ | | - | - |
| [56] | Ag / Graphene | 1.33 – 1.37 | 216 | 3,700 | $2.7\times10^{-5}$ | $4.6*10^{-5}$ | - | - |
| [57] | Ag / Graphene/ $TiO_2$ | 1.32 – 1.38 | - | 8,750 | - | - | 346.5 | - |

| | | | | | | | | |
|---|---|---|---|---|---|---|---|---|
| [58] | $Ag/TiO_2$ | 1.33 – 1.40 | 2245 | 10,300 | $9.71\times10^{-6}$ | $4.45*10^{-6}$ | 480 | - |
| [32] | AZO+Au | 1.27 – 1.42 | 8485.2 | 46,300 | $2.16\times10^{-6}$ | $1.18*10^{-6}$ | - | 16,500 |
| [34] | GZO+Au | 1.30 – 1.40 | | 11,480 | $8.71\times10^{-6}$ | | - | 11,720 |
| [35] | AZO+GZO | 1.30 – 1.41 | 11609.67 | 11,088.5 | $9.874\times10^{-6}$ | $8.61*10^{-7}$ | 1558.8 | 10,890.35 |
| [33] | GZO+Ag | 1.27 – 1.41 | 875.72 | 27,360 | $1.142\times10^{-5}$ | $3.65*10^{-6}$ | 243.4 | 27,341.5 |
| Our Work | ITO+ $Ag/TiO_2$ | 1.32-1.38 | 1668.34 | 50,652 | $1.97\times10^{-6}$ | $5.99\times10^{-6}$ | 1017.1 | 50,000 |

Table 8.2 makes it clear that our sensor is a perfect combination of outstanding sensing parameters. Additionally, it attains the highest DPSS value ever recorded, confirming the superiority of our sensor.

# Chapter 9

# Fabrication of the Proposed Sensor

## 9.1 Introduction

Our sensor is made using well-established methods for creating Photonic Crystal Fiber (PCF) structures. It has a unique wheel-shaped shape with three air holes curved like arcs. Below is a breakdown of the concepts of our sensor's potential fabrication steps.

### *9.1.1 Stack and Draw Method*

A common technique for creating Photonic Crystal Fiber (PCF) structures is the stack-and-draw method. Using this technique, glass tubes with the appropriate patterns of arc-shaped air holes are made, stacked to create a preform, and then drawn into a fiber. The chosen shape is preserved throughout the drawing process, guaranteeing that the complex structures needed for our sensor are faithfully mirrored in the finished fiber.

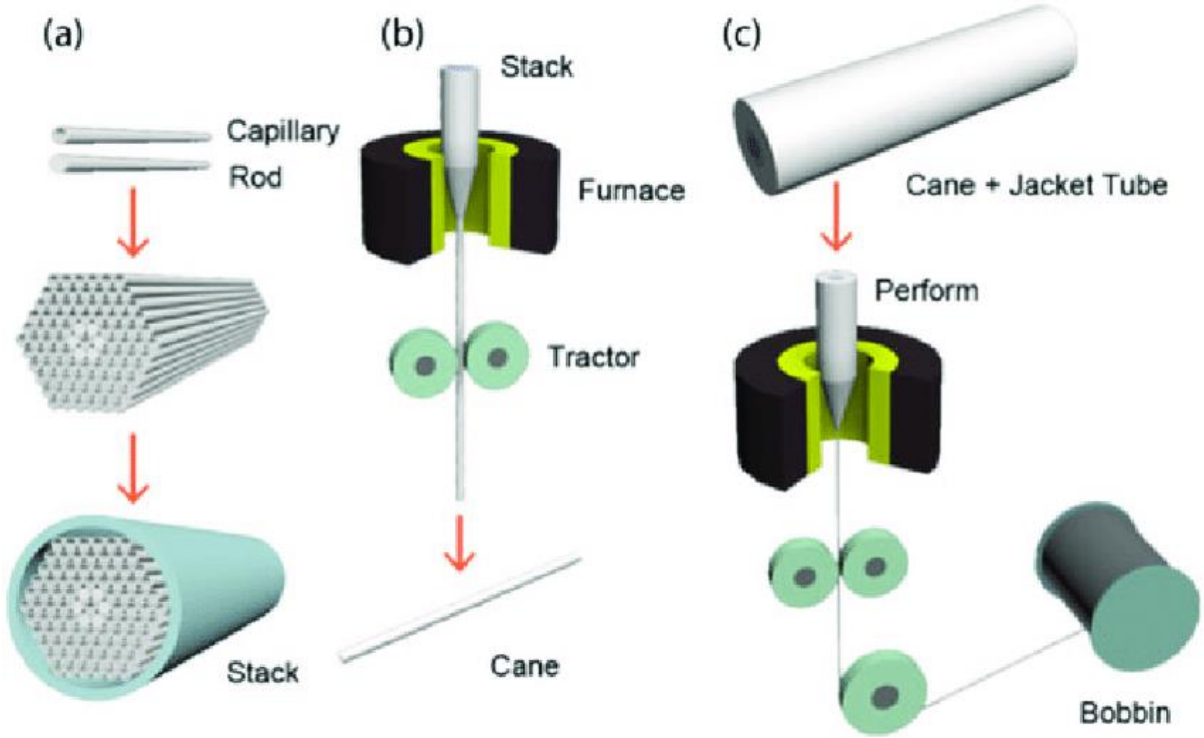


**Figure 9.1:** A brief schematic overview of the Stack and Draw Method

### *9.1.2 CNC Drilling*

Alternatively, a Computer Numerical Control (CNC) drilling machine can be used to define the sensor's structure. The precise geometries required for the air holes and other structural elements are drilled using this equipment. The arc-like forms and complex designs are precisely realized thanks to the precision provided by CNC drilling, giving the sensor a high degree of structural stability.

### *9.1.3 Double Step Photolithography Method*

The sensor's plasmonic layers are integrated using a two-step photolithography process. The first stage is to use Chemical Vapor Deposition (CVD) to deposit a plasmonic layer on the fiber's outside. This procedure guarantees that materials like ITO, silver, and TiO2 are coated uniformly and adherently. In order to precisely deposit the plasmonic layers, the selected portions of the fiber are covered with a mask in the second phase.

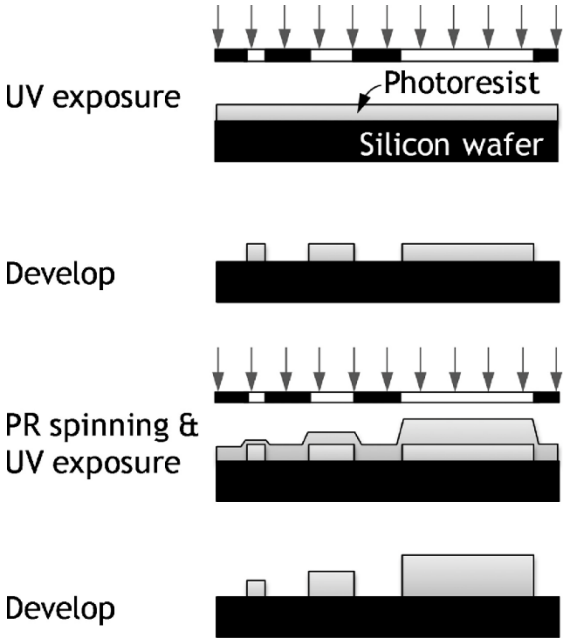


**Figure 9.2:** A brief overview of 2 step Photolithography Process

### *9.1.4 Chemical Vapor Deposition*

The CVD process is essential to the double-step photolithography process because it makes it easier to coat the fiber with plasmonic compounds. The size of the plasmonic layers allow them to be easily included into the PCF framework. Also, the air holes are enough in size to ensure that the plasmonic layers are well included, which ensures optimal functioning of the sensor.

## 9.2 Fabrication Steps of Our Sensor

Our sensor may be created with great precision and reliability by using these sophisticated fabrication techniques, guaranteeing that it satisfies the demanding specifications for its intended applications.

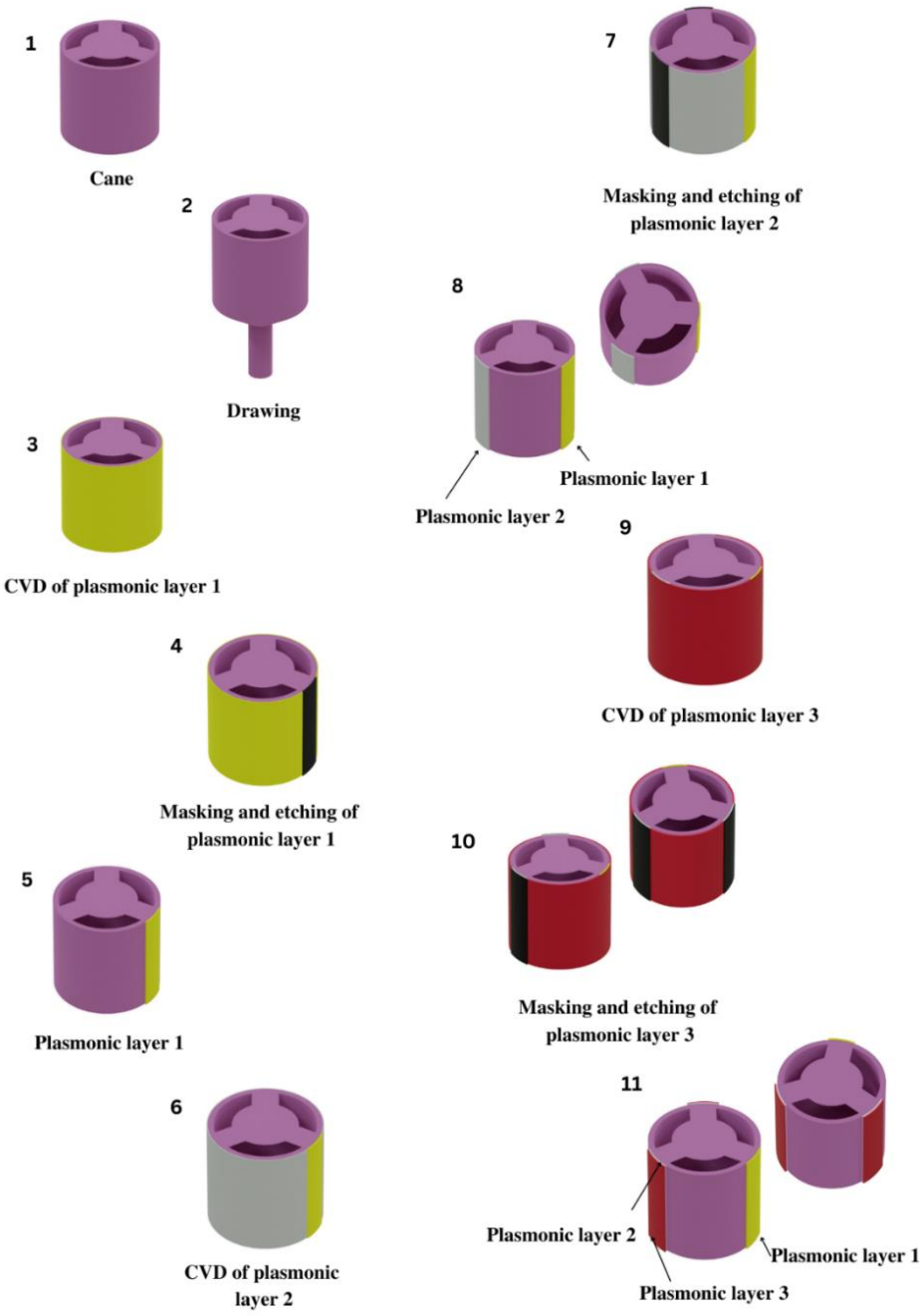


**Figure 9.3:** Prospective Steps of Fabrication of our Sensor

One common technique for creating PCFs is stack-and-draw method, which is used to design the geometry of the sensor [45]. In order to maintain the specified geometry, glass tubes with

the appropriate arc-like air hole patterns must be made, stacked, and then drawn into a fiber. The precise geometry needed to define the sensor's structure can likewise be drilled out using a CNC drilling machine [46].

A 2 step photolithography technique can be used to incorporate plasmonic layers. First stage is to use Chemical Vapor Deposition (CVD) to deposit a plasmonic layer on the fiber's outside [47]. The plasmonic layers can be precisely deposited in the following phase by using a mask to cover particular areas.

ITO, silver, and $TiO_2$ layers can be applied around the drawn cane using this technique. The wide air holes ensure optimal inclusion, and the plasmonic layers are designed to blend in seamlessly with the PCF utilizing the CVD process.

# Chapter 10

# Conclusion and Future Workplan

## 10.1 Conclusion

To sum up, our sensor has strong performance features, wide spectral coverage, and high sensitivity, making it a significant achievement in the field of plasmonic sensors. Utilizing custom-made plasmonic layers in conjunction with innovative PCF architectures has made it possible to achieve previously unattainable sensing capacities throughout a vast range of wavelengths and refractive indices. We believe that our sensor will find many uses in optical sensing, telecommunications, and other fields as we continue to research and develop it, advancing both science and technology.

We see a time when real-time, high-precision sensing solutions for a wide range of industrial, medicinal, and environmental problems are made possible in large part by our sensor. We want to further develop and enhance the capabilities of our sensor platform through continued research and cooperation, opening up new avenues for impact and innovation.

## 10.2 Future Direction

- To optimize sensitivity (DPSS and AS) and resolution (WS and FOM), plasmonic layers (such as TiO2/Au/Ag) should have their composition and thickness further refined.

- To examine how to combine several plasmonic materials (such as TiO2/Au/Graphene) in a single sensor to take advantage of synergistic effects and improve sensing parameters.

- To utilize the sensor's broad spectrum phase matching capacity to customise sensor designs and functionalisation procedures for distinct biomolecular detection applications.

- Provide sensor arrangements that are best suited for environmental monitoring, which includes contaminant and pollutant detection.

# Chapter 11

# Demonstration of Outcome Based Education (OBE)

## 11.1 Addressing COs and POs

The following table shows the COs for EEE 4700/4800 (Project and Thesis).

| COs | CO Statement | POs |
|---|---|---|
| **CO1** | Identify a contemporary real life problem related to electrical and electronic engineering by reviewing and analyzing existing research works. | PO2 |
| **CO2** | Determine functional requirements of the problem considering feasibility and efficiency through analysis and synthesis of information. | PO4 |
| **CO3** | Select a suitable solution and determine its method considering professional ethics, codes and standards. | PO8 |
| **CO4** | Adopt modern engineering resources and tools for the solution of the problem. | PO5 |
| **CO5** | Prepare management plan and budgetary implications for the solution of the problem. | PO11 |
| **CO6** | Analyze the impact of the proposed solution on health, safety, culture and society. | PO6 |
| **CO7** | Analyze the impact of the proposed solution on environment and sustainability. | PO7 |
| **CO8** | Develop a viable solution considering health, safety, cultural, societal and environmental aspects. | PO3 |
| **CO9** | Work effectively as an individual and as a team member for the accomplishment of the solution. | PO9 |
| **CO10** | Prepare various technical reports, design documentation, and deliver effective presentations for demonstration of the solution. | PO10 |
| **CO11** | Recognize the need for continuing education and participation in professional societies and meetings. | PO12 |

**Table 11.1**

The following table shows the aspects addressed for certain Program Outcomes (POs) addressed in EEE 4700/4800 for Project and Thesis.

| | Statement | Different Aspects | Put Tick ( √ ) |
|---|---|---|---|
| **PO2** | **Problem analysis:** Identify, formulate, research literature and analyse complex electrical and electronic engineering problems reaching substantiated conclusions using first principles of mathematics, natural sciences and engineering sciences. | | √ |
| **PO3** | **Design/development of solutions**: Design solutions for complex electrical and electronic engineering problems and design systems, components or processes that meet specified needs with appropriate consideration for public health and safety, cultural, societal, and environmental considerations. | Public health | √ |
| | | Safety | √ |
| | | Cultural | |
| | | Societal | √ |
| | | Environmental | √ |
| **PO4** | **Investigation:** Conduct investigations of complex electrical and electronic engineering problems using research-based knowledge and research methods including design of experiments, analysis and interpretation of data, and synthesis of information to provide valid conclusions. | Design of experiments | √ |
| | | Analysis and interpretation of data | √ |
| | | Synthesis of information | √ |
| **PO6** | **The engineer and society:** Apply reasoning informed by contextual knowledge to assess societal, health, safety, legal and cultural issues and the consequent responsibilities relevant to professional engineering practice and solutions to complex electrical and electronic engineering problems. | Societal | |
| | | Health | √ |
| | | Safety | √ |
| | | Legal | √ |
| | | Cultural | |

| | | | |
|---|---|---|---|
| **PO7** | **Environment and sustainability:** Understand and evaluate the sustainability and impact of professional engineering work in the solution of complex electrical and electronic engineering problems in societal and environmental contexts. | Societal | √ |
| | | Environmental | √ |
| **PO8** | **Ethics:** Apply ethical principles embedded with religious values, professional ethics and responsibilities, and norms of electrical and electronic engineering practice. | Religious values | |
| | | Professional ethics and responsibilities | √ |
| | | Norms | √ |
| **PO9** | **Individual work and teamwork:** Function effectively as an individual, and as a member or leader in diverse teams and in multi-disciplinary settings. | Individual | √ |
| | | Teamwork | √ |
| **PO10** | **Communication:** Communicate effectively on complex engineering activities with the engineering community and with society at large, such as being able to comprehend and write effective reports and design documentation, make effective presentations, and give and receive clear instructions. | Comprehend and write effective reports | √ |
| | | Design documentation | √ |
| | | Make effective presentations | √ |
| | | Give and receive clear instructions | √ |
| **PO11** | **Project management and finance:** Demonstrate knowledge and understanding of engineering management principles and economic decision-making and apply these to one's own work, as a member and leader in a team, to manage projects and in multidisciplinary environments. | Engineering management principles | √ |
| | | Economic decision-making | √ |
| | | Manage projects | √ |
| | | Multidisciplinary environments | √ |

**Table 11.2**

The following table explains or justifies how the COs and corresponding POs have been addressed in EEE 4700/4800 (Project and Thesis).

| COs | POs | Explanation/Justification |
|---|---|---|
| **CO1** | **PO2** | The core aspect is to propose a novel process / technology / model that addresses a previously unaddressed issue or declining innovation.<br>A Surface Plasmon Resonance in Photonic Crystal Fiber (SPR-PCF) sensor, which is designed with a theoretical photonics framework, can help address the challenge of biomolecule detection in medical science by providing fast and accurate sensing, which is essential for the identification and diagnosis of medical issues. |
| **CO2** | **PO4** | Conduction of information generation, analysis and post-judgment of effectiveness is also at the heart of the core objective.<br>In order to provide effective and quick detection, functional requirements include improving Surface Plasmon Resonance in Photonic Crystal Fiber (SPR-PCF) sensor sensors to detect and identify certain biomolecules based on refractive index values. |
| **CO3** | **PO8** | The proposed work addresses pertinent issues to enhance the effectiveness of the work in real life.<br>By inserting the sample into a PCF sensor and monitoring SPR and SPP activity through transmitted light, biomolecule detection is accomplished through the use of unique refractive index values, assuring ethical adherence to professional norms and codes. |
| **CO4** | **PO5** | Adoption of modern engineering resources and tools, COMSOL Multiphysics, for simulation and optimization of the proposed sensor to validate the sensor's practicality in real-life scenarios. |
| **CO5** | **PO11** | Likely issues related to execution, management (convenience of fabrication) and budgetary implications (material costing) for the proposed work are to be addressed with utmost priority |
| **CO6** | **PO6** | SPR-PCF sensors contribute to enhanced health diagnostics, rapid detection, improved safety measures, and cultural and societal benefits through advanced technologies and applications. |
| **CO7** | **PO7** | PCF sensor's compact design reduces production-related environmental effect, and reusable design improves sustainability for a range of SPR-PCF sensor applications. |

| | | |
|---|---|---|
| **CO8** | **PO3** | Using SPR-PCFs, we create biosensors that enable quick identification of health issues, guaranteeing an early diagnosis. We also expand the applications to environmental contamination detection, which encourages environmental sustainability, cultural sensitivity, and safety. |
| **CO9** | **PO9** | The team worked effectively both on individual and team basis for the accomplishment of the solution. |
| **CO10** | **PO10** | Various technical reports, design documentation, and delivery of effective presentations are established for demonstration of the solution |
| **CO11** | **PO12** | The team consciously recognizes the need for continuing education and participation in professional societies and meetings for further enhancement in the respective field beyond the proposed work. We have already moved onto the path of presenting our work on research journals. |

**Table 11.3**

## 11.2 Addressing Knowledge Profiles (K1-K8)

The following table shows the Knowledge Profiles (K3 – K8) addressed in EEE 4700/4800 (Project and Thesis).

| K | Knowledge Profile (Attribute) | Put Tick ( √ ) |
|---|---|---|
| **K3** | A systematic, theory-based formulation of engineering fundamentals required in the engineering discipline | √ |
| **K4** | Engineering specialist knowledge that provides theoretical frameworks and bodies of knowledge for the accepted practice areas in the engineering discipline; much is at the forefront of the discipline | √ |
| **K5** | Knowledge that supports engineering design in a practice area | √ |
| **K6** | Knowledge of engineering practice (technology) in the practice areas in the engineering discipline | √ |
| **K7** | Comprehension of the role of engineering in society and identified issues in engineering practice in the discipline: ethics and the engineer's professional responsibility to public safety; the impacts of engineering activity; economic, social, cultural, environmental and sustainability | √ |
| **K8** | Engagement with selected knowledge in the research literature of the discipline | √ |

**Table 11.4**

The following table explains or justifies how the Knowledge Profiles (K3 – K8) have been addressed in EEE 4700/4800 (Project and Thesis).

| K | Explanation/Justification |
|---|---|
| **K3** | Recognizing the fundamental ideas behind Photonic Crystal Fiber (PCF) and Surface Plasmon Resonance (SPR) in order to detect biomolecules.<br>Using photonics frameworks to design SPR-PCF sensors will enable quick and precise biomolecule sensing, which is essential for medical diagnostics. |
| **K4** | SPR-PCF sensor optimization to identify particular biomolecules based on refractive index values, guaranteeing quick and effective identification for medical issue diagnosis. |
| **K5** | SPR-PCF sensors use specific refractive index values to identify biomolecules; for accurate detection, the behavior of core modes and SPP modes is observed via transmitted light. |
| **K6** | Using COMSOL Multiphysics to simulate and optimize SPR-PCF sensors, which will result in their actual manufacture and testing to confirm their functionality. |
| **K7** | Understanding the function of engineering in society and recognizing relevant issues within the engineering practice, including ethical considerations and the engineer's obligation to ensure public safety were/are employed all along the process |
| **K8** | Designing, optimizing, and fabricating sensors by utilizing existing research in photonics, biosensors, and SPR-PCF technologies allows one to contribute to academic research and conference presentations that demonstrate progress in SPR-PCF sensor technology and good outcomes. |

**Table 11.5**

## 11.3 Addressing Attributes of Ranges of Complex Engineering Problem Solving (P1 – P7)

The following table shows the attributes of ranges of Complex Engineering Problem Solving (P1 – P7) addressed in EEE 4700/4800 (Project and Thesis).

| P | Range of Complex Engineering Problem Solving | Put Tick ( √ ) |
|---|---|---|
| **Attribute** | Complex Engineering Problems have characteristic P1 and some or all of P2 to P7: | |
| Depth of knowledge required | **P1:** Cannot be resolved without in-depth engineering knowledge at the level of one or more of K3, K4, K5, K6 or K8 which allows a fundamentals-based, first principles analytical approach | √ |

| | | |
|---|---|---|
| Range of conflicting requirements | **P2:** Involve wide-ranging or conflicting technical, engineering and other issues | √ |
| Depth of analysis required | **P3:** Have no obvious solution and require abstract thinking, originality in analysis to formulate suitable models | √ |
| Familiarity of issues | **P4:** Involve infrequently encountered issues | √ |
| Extent of applicable codes | **P5:** Are outside problems encompassed by standards and codes of practice for professional engineering | √ |
| Extent of stakeholder involvement and conflicting requirements | **P6:** Involve diverse groups of stakeholders with widely varying needs | √ |
| Interdependence | **P7:** Are high level problems including many component parts or sub-problems | √ |

**Table 11.6**

The following table explains or justifies how the attributes of ranges of Complex Engineering Problem Solving (P1 – P7) have been addressed in EEE 4700/4800 (Project and Thesis).

| P | Explanation/Justification |
|---|---|
| **P1** | Basic knowledge of photonics and electromagnetics were acquired and applied (K3, K4), design and application knowledge were acquired and applied and multiple papers were reviewed. |
| **P2** | Conflicting requirements in terms of achieving high sensor sensitivity while balancing fabrication feasibility and tolerance to imperfections were addressed by issuing wide-ranging technical design considerations, fabrication methods, numerical modeling, and sensor sensitivity optimization. |
| **P3** | Utilizing COMSOL Multiphysics to create novel methods and abstract models (K4, K6) for SPR-PCF sensor simulation and optimization. |
| **P4** | Unique enhancement of sensor sensitivity through unique geometrical parameters and specific combination of plasmonic materials (K5). |
| **P5** | A wide range of considerations, including external factors like environmental, societal, and regulatory concerns encompassed by the engineering standards and codes of practice are followed (K7). |

| | |
|---|---|
| **P6** | Diverse groups of stakeholders like the healthcare society (doctors & patients) and researchers are involved, through our research of those industry (healthcare, material cience etc.) (K7). |
| **P7** | Using multidisciplinary knowledge from COMSOL software environment, material sciences, biosensing, and photonics (K3, K4, K6) to create, test, and validate SPR-PCF sensors holistically for a range of applications. |

**Table 11.7**

## 11.4 Addressing Attributes of Ranges of Complex Engineering Activities (A1 – A5)

The following table shows the attributes of ranges of Complex Engineering Activities (A1 – A5) addressed in EEE 4700/4800 (Project and Thesis).

| **A** | **Range of Complex Engineering Activities** | **Put Tick ( √ )** |
|---|---|---|
| **Attribute** | Complex activities means (engineering) activities or projects that have some or all of the following characteristics: | |
| Range of resources | **A1:** Involve the use of diverse resources (and for this purpose resources include people, money, equipment, materials, information and technologies) | √ |
| Level of interaction | **A2:** Require resolution of significant problems arising from interactions between wide-ranging or conflicting technical, engineering or other issues | √ |
| Innovation | **A3:** Involve creative use of engineering principles and research-based knowledge in novel ways | √ |
| Consequences for society and the environment | **A4:** Have significant consequences in a range of contexts, characterized by difficulty of prediction and mitigation | √ |
| Familiarity | **A5:** Can extend beyond previous experiences by applying principles-based approaches | √ |

**Table 11.8**

The following table explains or justifies how the attributes of ranges of Complex Engineering Activities (A1 – A5) have been addressed in EEE 4700/4800 (Project and Thesis).

| A | Explanation/Justification |
|---|---|
| **A1** | Diverse resources like people (thesis team of students with supervisor, specialist and consultants), money, materials (different software platforms), information and technologies are involved. |
| **A2** | Resolution of significant problems arising from interactions between wide-ranging or conflicting technical, engineering or other issues are achieved by making design considerations, fabrication, and sensor optimization of different parameters. |
| **A3** | Pre-existing engineering principles, research-based knowledge, creative engineering thinking are used to create more sensitive PCF in novel ways. |
| **A4** | Have significant consequences as the real-life application of this invention will be a ground-breaking invention in the world of diagnostics. |
| **A5** | Going beyond traditional methods for developing sensors by using principles-based engineering techniques. By utilizing knowledge from previous studies, simulations, and optimization strategies, you can effectively design, fabricate, and test the SPR-PCF sensor system. |

**Table 11.9**

# References


[1] C. Di Primo, “Surface Plasmon Resonance for Investigating Molecular Interactions with RNA,” 2020, pp. 73–88. doi: 10.1007/978-1-0716-0278-2_6.

[2] M. R. Islam *et al.*, “Surface plasmon resonance based highly sensitive gold coated PCF biosensor,” *Applied Physics A*, vol. 127, no. 2, p. 118, Feb. 2021, doi: 10.1007/s00339-020-04162-5.

[3] M. R. Islam *et al.*, “Highly birefringent gold-coated SPR sensor with extremely enhanced amplitude and wavelength sensitivity,” *The European Physical Journal Plus*, vol. 136, no. 2, p. 238, Feb. 2021, doi: 10.1140/epjp/s13360-021-01220-6.

[4] M. R. Islam *et al.*, “Design and Analysis of a Biochemical Sensor Based on Surface Plasmon Resonance with Ultra-high Sensitivity,” *Plasmonics*, vol. 16, no. 3, pp. 849–861, Jun. 2021, doi: 10.1007/s11468-020-01355-9.

[5] M. R. Islam *et al.*, “Design and analysis of a QC-SPR-PCF sensor for multipurpose sensing with supremely high FOM,” *Appl Nanosci*, vol. 12, no. 1, pp. 29–45, Jan. 2022, doi: 10.1007/s13204-021-02150-6.

[6] D. J. J. Hu and H. P. Ho, “Recent advances in plasmonic photonic crystal fibers: design, fabrication and applications,” *Adv Opt Photonics*, vol. 9, no. 2, p. 257, Jun. 2017, doi: 10.1364/AOP.9.000257.

[7] Md. A. Islam, M. R. Islam, A. M. Al Naser, F. Anzum, and F. Z. Jaba, “Square structured photonic crystal fiber based THz sensor design for human body protein detection,” *J Comput Electron*, vol. 20, no. 1, pp. 377–386, Feb. 2021, doi: 10.1007/s10825-020-01606-2.

[8] M. R. Islam, A. N. M. Iftekher, F. A. Mou, Md. M. Rahman, and M. I. H. Bhuiyan, “Design of a Topas-based ultrahigh-sensitive PCF biosensor for blood component detection,” *Applied Physics A*, vol. 127, no. 2, p. 109, Feb. 2021, doi: 10.1007/s00339-020-04261-3.

[9] Md. A. Islam, M. R. Islam, S. Siraz, M. Rahman, M. S. Anzum, and F. Noor, “Wheel structured Zeonex-based photonic crystal fiber sensor in THz regime for sensing milk,” *Applied Physics A*, vol. 127, no. 5, p. 311, May 2021, doi: 10.1007/s00339-021-04472-2.

[10] M. R. H. Khan, F. A. M. Ali, and M. R. Islam, “THz sensing of CoViD-19 disinfecting products using photonic crystal fiber,” *Sens Biosensing Res*, vol. 33, p. 100447, Aug. 2021, doi: 10.1016/j.sbsr.2021.100447.

[11] Md. M. Rahman, F. A. Mou, M. I. H. Bhuiyan, and M. R. Islam, “Refractometric THz Sensing of Blood Components in a Photonic Crystal Fiber Platform,” *Brazilian Journal of Physics*, vol. 52, no. 2, p. 47, Apr. 2022, doi: 10.1007/s13538-022-01054-2.

[12] C. M. B. Cordeiro *et al.*, "Microstructured-core optical fibre for evanescent sensing applications," *Opt Express*, vol. 14, no. 26, p. 13056, 2006, doi: 10.1364/OE.14.013056.

[13] T. M. Monro, W. Belardi, K. Furusawa, J. C. Baggett, N. G. R. Broderick, and D. J. Richardson, "Sensing with microstructured optical fibres," *Meas Sci Technol*, vol. 12, no. 7, pp. 854–858, Jul. 2001, doi: 10.1088/0957-0233/12/7/318.

[14] Md. A. Islam, M. R. Islam, Z. Tasnim, R. Islam, R. L. Khan, and E. Moazzam, "Low-Loss and Dispersion-Flattened Octagonal Porous Core PCF for Terahertz Transmission Applications," *Iranian Journal of Science and Technology, Transactions of Electrical Engineering*, vol. 44, no. 4, pp. 1583–1592, Dec. 2020, doi: 10.1007/s40998-020-00337-1.

[15] M. R. Islam, A. N. M. Iftekher, F. Noor, M. R. H. Khan, Md. T. Reza, and M. M. Nishat, "AZO-coated plasmonic PCF nanosensor for blood constituent detection in near-infrared and visible spectrum," *Applied Physics A*, vol. 128, no. 1, p. 86, Jan. 2022, doi: 10.1007/s00339-021-05220-2.

[16] W. L. Barnes, A. Dereux, and T. W. Ebbesen, "Surface plasmon subwavelength optics," *Nature*, vol. 424, no. 6950, pp. 824–830, Aug. 2003, doi: 10.1038/nature01937.

[17] D. Paul and R. Biswas, "Highly sensitive LSPR based photonic crystal fiber sensor with embodiment of nanospheres in different material domain," *Opt Laser Technol*, vol. 101, pp. 379–387, May 2018, doi: 10.1016/j.optlastec.2017.11.040.

[18] C. Zhou, "Localized surface plasmonic resonance study of silver nanocubes for photonic crystal fiber sensor," *Opt Lasers Eng*, vol. 50, no. 11, pp. 1592–1595, Nov. 2012, doi: 10.1016/j.optlaseng.2012.05.020.

[19] Md. A. Mollah and Md. S. Islam, "Novel Single Hole Exposed-Suspended Core Localized Surface Plasmon Resonance Sensor," *IEEE Sens J*, pp. 1–1, 2020, doi: 10.1109/JSEN.2020.3023975.

[20] M. S. Aruna Gandhi, K. Senthilnathan, P. Ramesh Babu, and Q. Li, "Highly Sensitive Localized Surface Plasmon Polariton Based D-Type Twin-Hole Photonic Crystal Fiber Microbiosensor: Enhanced Scheme for SERS Reinforcement," *Sensors*, vol. 20, no. 18, p. 5248, Sep. 2020, doi: 10.3390/s20185248.

[21] J. Wu, S. Li, X. Wang, M. Shi, X. Feng, and Y. Liu, "Ultrahigh sensitivity refractive index sensor of a D-shaped PCF based on surface plasmon resonance," *Appl Opt*, vol. 57, no. 15, p. 4002, May 2018, doi: 10.1364/AO.57.004002.

[22] T. Li, L. Zhu, X. Yang, X. Lou, and L. Yu, "A Refractive Index Sensor Based on H-Shaped Photonic Crystal Fibers Coated with Ag-Graphene Layers," *Sensors*, vol. 20, no. 3, p. 741, Jan. 2020, doi: 10.3390/s20030741.

[23] S. M. Abu Sufian Sunny, T. Ahmed, A. Anzum, and A. K. Paul, “Performance Analysis of a PCF SPR Based Highly Sensitive Biosensor,” in *2019 IEEE International Conference on Biomedical Engineering, Computer and Information Technology for Health (BECITHCON)*, IEEE, Nov. 2019, pp. 7–10. doi: 10.1109/BECITHCON48839.2019.9063192.

[24] Md. N. Hossen, Md. Ferdous, Md. Abdul Khalek, S. Chakma, B. K. Paul, and K. Ahmed, “Design and analysis of biosensor based on surface plasmon resonance,” *Sens Biosensing Res*, vol. 21, pp. 1–6, Nov. 2018, doi: 10.1016/j.sbsr.2018.08.003.

[25] Md. R. Hasan *et al.*, “Spiral Photonic Crystal Fiber-Based Dual-Polarized Surface Plasmon Resonance Biosensor,” *IEEE Sens J*, vol. 18, no. 1, pp. 133–140, Jan. 2018, doi: 10.1109/JSEN.2017.2769720.

[26] J. Lv *et al.*, “Numerical Analysis of Multifunctional Biosensor with Dual-Channel Photonic Crystal Fibers Based on Localized Surface Plasmon Resonance,” *Coatings*, vol. 12, no. 6, p. 742, May 2022, doi: 10.3390/coatings12060742.

[27] G. Xiao *et al.*, “Fiber Optic Sensor with a Gold Nanowire Group Array for Broad Range and Low Refractive Index Detection,” *Photonics*, vol. 9, no. 9, p. 661, Sep. 2022, doi: 10.3390/photonics9090661.

[28] A. K. Shakya and S. Singh, “Design and analysis of dual polarized Au and TiO2-coated photonic crystal fiber surface plasmon resonance refractive index sensor: an extraneous sensing approach,” *J Nanophotonics*, vol. 15, no. 01, Feb. 2021, doi: 10.1117/1.JNP.15.016009.

[29] A. A. Rifat, G. A. Mahdiraji, Y. M. Sua, R. Ahmed, Y. G. Shee, and F. R. M. Adikan, “Highly sensitive multi-core flat fiber surface plasmon resonance refractive index sensor,” *Opt Express*, vol. 24, no. 3, p. 2485, Feb. 2016, doi: 10.1364/OE.24.002485.

[30] H. Yang, G. Wang, Y. Lu, and J. Yao, “Highly sensitive refractive index sensor based on SPR with silver and titanium dioxide coating,” *Opt Quantum Electron*, vol. 53, no. 6, p. 341, Jun. 2021, doi: 10.1007/s11082-021-02981-1.

[31] S. Singh and Y. K. Prajapati, “TiO2/gold-graphene hybrid solid core SPR based PCF RI sensor for sensitivity enhancement,” *Optik (Stuttg)*, vol. 224, p. 165525, Dec. 2020, doi: 10.1016/j.ijleo.2020.165525.

[32] M. Rakibul Islam, A. N. M. Iftekher, M. S. Anzum, M. Rahman, and S. Siraz, “LSPR Based Double Peak Double Plasmonic Layered Bent Core PCF-SPR Sensor for Ultra-Broadband Dual Peak Sensing,” *IEEE Sens J*, vol. 22, no. 6, pp. 5628–5635, Mar. 2022, doi: 10.1109/JSEN.2022.3149715.

[33] M. R. Islam, A. N. M. Iftekhar, A. A. Hassan, S. Zaman, and M. A. Al Hosain, “Double plasmonic peak shift sensitivity: an analysis of a highly sensitive LSPR-PCF sensor for a

diverse range of analyte detection," *Applied Physics A*, vol. 129, no. 8, p. 571, Aug. 2023, doi: 10.1007/s00339-023-06851-3.

[34] M. R. Islam, A. N. M. Iftekher, M. F. Etu, W. R. Rashmi, and S. Abbas, "Dual Peak Double Resonance Sensing Using a Dual Plasmonic Material PCF-SPR Sensor," *Plasmonics*, vol. 18, no. 3, pp. 983–993, Jun. 2023, doi: 10.1007/s11468-023-01829-6.

[35] M. R. Islam, A. N. M. Iftekher, I. Marshad, N. F. Rity, and R. U. Ahmad, "Analysis of a dual peak dual plasmonic layered LSPR-PCF sensor – Double peak shift sensitivity approach," *Optik (Stuttg)*, vol. 280, p. 170793, Jun. 2023, doi: 10.1016/j.ijleo.2023.170793.

[36] G. V. Naik and A. Boltasseva, "Semiconductors for plasmonics and metamaterials," *physica status solidi (RRL) - Rapid Research Letters*, vol. 4, no. 10, pp. 295–297, Oct. 2010, doi: 10.1002/pssr.201004269.

[37] G. V. Naik, V. M. Shalaev, and A. Boltasseva, "Alternative Plasmonic Materials: Beyond Gold and Silver," *Advanced Materials*, vol. 25, no. 24, pp. 3264–3294, Jun. 2013, doi: 10.1002/adma.201205076.

[38] C. Liu *et al.*, "Surface plasmon resonance (SPR) infrared sensor based on D-shape photonic crystal fibers with ITO coatings," *Opt Commun*, vol. 464, p. 125496, Jun. 2020, doi: 10.1016/j.optcom.2020.125496.

[39] P. R. West, S. Ishii, G. V. Naik, N. K. Emani, V. M. Shalaev, and A. Boltasseva, "Searching for better plasmonic materials," *Laser Photon Rev*, vol. 4, no. 6, pp. 795–808, Nov. 2010, doi: 10.1002/lpor.200900055.

[40] P. B. Johnson and R. W. Christy, "Optical Constants of the Noble Metals," *Phys Rev B*, vol. 6, no. 12, pp. 4370–4379, Dec. 1972, doi: 10.1103/PhysRevB.6.4370.

[41] T. Wieduwilt *et al.*, "Ultrathin niobium nanofilms on fiber optical tapers – a new route towards low-loss hybrid plasmonic modes," *Sci Rep*, vol. 5, no. 1, p. 17060, Nov. 2015, doi: 10.1038/srep17060.

[42] L. Zhou *et al.*, "Irreversible accumulated SERS behavior of the molecule-linked silver and silver-doped titanium dioxide hybrid system," *Nat Commun*, vol. 11, no. 1, p. 1785, Apr. 2020, doi: 10.1038/s41467-020-15484-6.

[43] T. Wang *et al.*, "The effect of the TiO2 film on the performance of the optical fiber SPR sensor," *Opt Commun*, vol. 448, pp. 93–97, Oct. 2019, doi: 10.1016/j.optcom.2019.05.023.

[44] S. Selvendran, J. Divya, A. Sivanantha Raja, A. Sivasubramanian, and S. Itapu, "A Reconfigurable Surface-Plasmon-Based Filter/Sensor Using D-Shaped Photonic Crystal Fiber," *Micromachines (Basel)*, vol. 13, no. 6, p. 917, Jun. 2022, doi: 10.3390/mi13060917.

[45] D. Pysz *et al.*, “Stack and draw fabrication of soft glass microstructured fiber optics,” *Bulletin of the Polish Academy of Sciences Technical Sciences*, vol. 62, no. 4, pp. 667–682, Dec. 2014, doi: 10.2478/bpasts-2014-0073.

[46] S. Choi and J.-K. Park, “Two-step photolithography to fabricate multilevel microchannels,” *Biomicrofluidics*, vol. 4, no. 4, p. 046503, Dec. 2010, doi: 10.1063/1.3517230.

[47] P. J. A. Sazio *et al.*, “Microstructured Optical Fibers as High-Pressure Microfluidic Reactors,” *Science (1979)*, vol. 311, no. 5767, pp. 1583–1586, Mar. 2006, doi: 10.1126/science.1124281.

[48] M. R. Islam *et al.*, “Design and numerical analysis of a gold-coated photonic crystal fiber based refractive index sensor,” *Opt Quantum Electron*, vol. 53, no. 2, p. 112, Feb. 2021, doi: 10.1007/s11082-021-02748-8.

[49] H. Ahmad *et al.*, “Wide-band fanned-out supercontinuum source covering O-, E-, S-, C-, L- and U-bands,” *Opt Laser Technol*, vol. 44, no. 7, pp. 2168–2174, Oct. 2012, doi: 10.1016/j.optlastec.2012.03.007.

[50] B. K. Paul, Md. S. Islam, K. Ahmed, and S. Asaduzzaman, “Alcohol sensing over O+E+S+C+L+U transmission band based on porous cored octagonal photonic crystal fiber,” *Photonic Sensors*, vol. 7, no. 2, pp. 123–130, Jun. 2017, doi: 10.1007/s13320-017-0376-6.

[51] R. Stanley, “Plasmonics in the mid-infrared,” *Nat Photonics*, vol. 6, no. 7, pp. 409–411, Jul. 2012, doi: 10.1038/nphoton.2012.161.

[52] R. Soref, “Mid-infrared photonics in silicon and germanium,” *Nat Photonics*, vol. 4, no. 8, pp. 495–497, Aug. 2010, doi: 10.1038/nphoton.2010.171.

[53] V. Kaur and S. Singh, “Design of D-Shaped PCF-SPR sensor with dual coating of ITO and ZnO conducting metal oxide,” *Optik (Stuttg)*, vol. 220, p. 165135, Oct. 2020, doi: 10.1016/j.ijleo.2020.165135.

[54] M. F. O. Hameed, S. S. A. Obayya, K. Al-Begain, A. M. Nasr, and M. I. Abo el Maaty, “Accurate radial basis function based neural network approach for analysis of photonic crystal fibers,” *Opt Quantum Electron*, vol. 40, no. 11–12, pp. 891–905, Sep. 2008, doi: 10.1007/s11082-009-9290-5.

[55] X. Yang, Y. Lu, B. Liu, and J. Yao, “Analysis of Graphene-Based Photonic Crystal Fiber Sensor Using Birefringence and Surface Plasmon Resonance,” *Plasmonics*, vol. 12, no. 2, pp. 489–496, Apr. 2017, doi: 10.1007/s11468-016-0289-z.

[56] J. N. Dash and R. Jha, “On the Performance of Graphene-Based D-Shaped Photonic Crystal Fibre Biosensor Using Surface Plasmon Resonance,” *Plasmonics*, vol. 10, no. 5, pp. 1123–1131, Oct. 2015, doi: 10.1007/s11468-015-9912-7.

[57] D. Wang *et al.*, “High-Performance Tapered Fiber Surface Plasmon Resonance Sensor Based on the Graphene/Ag/TiO2 Layer,” *Plasmonics*, vol. 16, no. 6, pp. 2291–2303, Dec. 2021, doi: 10.1007/s11468-021-01483-w.

[58] H. Fang, C. Wei, H. Yang, B. Zhao, L. Yuan, and J. Li, “D-Shaped Photonic Crystal Fiber Plasmonic Sensor Based on Silver-Titanium Dioxide Composite Micro-grating,” *Plasmonics*, vol. 16, no. 6, pp. 2049–2059, Dec. 2021, doi: 10.1007/s11468-021-01468-9.